# Supporting information: Thiazole-Linked Covalent Organic Frameworks for Enhanced Photoreductive Gold Recovery from E-waste

Gilles Matthys[a], Andreas Laemont[a], Diem Van Hamme[a], Wafaa Ahmed Mohamed[a], Laurens Bourda[a,b], Rundong Wang[a], Karen Leus[c], Natalie De Geyter[c], Rino Morent[c], Roy Lavendomme[d] , Pascal Van Der Voort[a]

[a] Gilles Matthys, Andreas Laemont, Diem Van Hamme, Rundong Wang, Wafaa Ahmed Mohammed, Pascal Van Der Voort
Center for Ordered Materials, Organometallics and Catalysis (COMOC)
Department of Chemistry, Ghent University
Krijgslaan 281- S3, 9000 Ghent, Belgium

[b] Laurens Bourda
Department of Chemistry, KU Leuven
Celestijnenlaan 200 F, 3001 Leuven

[c] Nathalie De Geyter, Rino Morent, Karen Leus
Research Unit Plasma Technology (RUPT)
Department of Applied Physics, Ghent University
Sint-Pietersnieuwstraat 41, B4, 9000 Ghent, Belgium

[d] Roy Lavendomme
Laboratoire de Chimie Organique & Laboratoire de Résonance Magnétique Nucléaire Haute Résolution
Université libre de Bruxelles (ULB)
Avenue F. D. Roosevelt 50, CP160/06-08, B-1050 Brussels, Belgium

## 1. General information

### 1.1 Materials

1,4 Dioxane (Chem-Lab, ≥ 99%), n-Butanol (n-BuOH, Chem-Lab, 99.9%), Hydrochloric acid (HCl, Sigma-Aldrich, Reagent grade 37%), Acetic Acid (AcOH, Chem-Lab, 99.8%), Methanol (MeOH, Chem-Lab, ≥ 99%), Ethanol (EtOH, Chem-Lab), Acetone (Chem-Lab), Potassium carbonate ($K_2CO_3$, Sigma-Aldrich), Chlorform-d ($CDCl_3$, Eurisotop, 99.8%), Dimethylsulfoxide-$d_6$ (DMSO-$d_6$, Eurisotop, 99.8%), Potassium tetrachloroaurate(III) (KAuCl4, BLD Pharm, 98%), 1,3,5-Tris(4-aminophenyl)benzene (TAPB, BLD Pharm, 97%), Sulfur (Sigma-Aldrich, ≥ 99%), 1,4-Dichlorobenzene (TCI, ≥ 99%), 1,2-Dichlorobenzene (TCI, ≥ 99%), 1,4-Phenylenediamine (TCI, ≥ 98%), Cyanuric Chloride (TCI, ≥ 98%), N,N-Dimethylformadide (DMF, Chem-Lab, ≥ 99%), Copper(II) acetate monohydrate (TCI, ≥ 95%), Sodium Azide (TCI, ≥ 99%), 4-formylbenzonitrile (BLD Pharm, 97%), [1,1'-Bis(diphenylphosphino)ferrocene]dichloropalladium(II) ($Pd(dppf)Cl_2$, BLD Pharm, 98%), 4-Formylphenylboronic acid (BLD Pharm, 98%), 1,3,6,8-Tetrabromopyrene (BLD Pharm, 95%).

### 1.2 Instrumentation

**Nuclear Magnetic Resonance Spectroscopy (NMR)**

NMR spectra were recorded at 7.0 Tesla (Bruker Avance I). Solvent signals were used for chemical shift referencing: Residual $^1H$ signal at 2.5 ppm for DMSO-$d_6$ and 7.26 ppm for $CDCl_3$. Abbreviations: s: singlet, d: doublet, dd: doublet of doublet.

**Nitrogen Sorption**

Nitrogen adsorption/desorption isotherms were measured at 77 K on an Anton Paar Autosorb 6100. The samples were activated under vacuum at 120 °C overnight prior to measurement.

**Powder X-Ray Diffraction**

Powder X-ray diffraction (PXRD) patterns were collected on a Bruker D8 Advance diffractometer equipped with a Cu-$K_\alpha$ (l = 1.5405 Å) source, a goniometer and a Peltier cooled Si (Li) solid-state detector.

**Fourier-Transform Infrared Spectroscopy (FTIR)**

Measurements were recorded on a Perkin Elmer FTIR SPECTRUM 1000 spectrometer with Attenuated Total Reflection (ATR) with a PIKE Miracle ATR unit in a frequency range from 4000 to 600 $cm^{-1}$.

**Ultraviolet/Visible Light Spectroscopy (UV-Vis)**

UV-Vis spectra were recorded on Shimadzu UV 2600 Scanning Spectrophotometer having a stirring attachment.

**Transmission Electron Microscopy (TEM)**

Transmission Electron Microscopy (TEM) imaging was done on a JEOL JEM-1010 microscope at 100 kV without spherical aberration.

**Light setup**

The measurements involving light used the EvoluChem PhotoRedOx Box 34W white LED light.

**X-Ray Photoelectron Spectroscopy (XPS)**

The surface chemical composition of the samples was investigated by X-ray photoelectron spectroscopy (XPS) using the PHI 5000 VersaProbe II spectrometer equipped with a monochromatic Al Kα X-ray source (hν = 1486.6 eV). To do so, the samples were excited with an X-ray beam (size: 200 μm) over an area of 500 x 500 $\mu m^2$ at a power of 50 W. Wide range survey scans and high-resolution spectra were recorded with a pass energy of 187.85 eV and 23.5 eV and a step size of 0.8 eV and 0.1 eV respectively. All spectra were acquired at a take-off angle of 45° relative to the sample surface in the XPS chamber where the pressure was constantly maintained below $10^{-6}$ Pa.

**Thermogravimetric Analysis (TGA)**

Thermogravimetric analysis profiles were recorded on Perkin-Elmer STA6000, TGA analyzer under an air atmosphere with a heating rate of 10 °C/min.

**Electrochemical measurements (Mott-Shottky, Electrochemical Impedance Spectroscopy (EIS), Photocurrent response)**

3 mg of the photocatalysts were dispersed in a mixture containing 300 μL EtOH, and 30 μL Nafion. The mixture was sonicated for 4 hours to form a homogenous catalyst ink. 100 μL of this catalyst ink was drop-casted on a polished 1 cm × 2 cm area of an FTO glass and dried in air. These measurements were conducted on a CHI 660E electrochemical workstation in a three-electrode cell system under irradiation of with 300 W Xe lamp (Perfect Light PLS-SXE 300+) with a ≥ 420 nm cutoff filter. A Pt wire and a calomel electrode were used as the working electrode and the reference electrode, respectively. A 0.1 M $Na_2SO_4$ solution was utilized as electrolyte. Electrochemical impedance spectroscopy (EIS) was carried out at a bias potential of +1.5 V in the dark. Impedance spectra were fitted using the equivalent Randle circuit $R_s + (Q_{Bulk}/R_{Bulk}) + (Q_{CT}/R_{CT})$, where $R_s$ is the solvent resistance, $R_{Bulk}$ is the bulk resistance, and $R_{CT}$ is the charge transfer resistance. The Mott-Schottky measurement was performed at frequency of 1000, 2000, and 3000 Hz respectively in dark conditions.

**Inductive Coupled Plasma Optical Emission Spectroscopy (ICP-OES)**

Cu, Ni, and Zn were analyzed on Thermo Fisher iCap 7000. Cu was analyzed at 327.39 nm, Ni was analyzed at 341.47 nm, Zn analysis was done at 206.20 nm. The 3 elements were calibrated with standards 0 – 0.01 – 0.05 – 0.2 – 1 – 5 - 10 – 25 – 50 mg/L prepared from single 1000 mg/L stock solution of MERC Certipur. The calibration was verified with an independant standard of 2 mg/L prepared from a multi element stock standard of 100 mg/L (VWR Aristar 89166.180). Intenal standard correction was done with inline adding 10 µg/L Thorium.

**Inductive Coupled Plasma Mass Spectrometry (ICP-MS)**

ICP-MS measurements were performed on a NexION 300 (Perkin Elmer) apparatus, with gold analysis on mass 197 Dalton. The calibration was done with standards which are 0 – 1 – 5 – 20 – 100 µg/L prepared from a single 1000 mg/L stock solution (Chemlab, CL01.0731.0100). The calibration was verified with an independant standard of 20 µg/L prepared from a multi element stock standard of 10 mg/L (TraceCERT 41135-100 mL). Internal standard correction was by inline adding 10 µg/L Thorium.

## 2. Computational modelling

### 2.1.Geometry optimized structures

Intitial geometry optimization of COF structures was carried out using the Forcite module of BIOVIA Materials Studio 2017 (17.1.0.48) (Dassault Systèmes, San Diego, 2017) with the Universal Force Field (UFF).[1]

### 2.2.Pawley refinement

Pawley refinement of the PXRD patterns was carried out using the Reflex module of BIOVIA Materials Studio 2017 (17.1.0.48) (Dassault Systèmes, San Diego, 2017). The geometry optimized models of the COFs were used to provide starting unit cell parameters for refinement. The experimental PXRD patterns were refined from 2.0 to 40° in 2θ ($\lambda_{Copper}$ = 1.5405 Å), and peaks were fitted to Pseudo-Voigt peak profiles. The freely varying parameters set for the refinement were the full width at half maximum (FWHM) parameters U, V, W from the Caglioti formula (describing peak broadening), the profile parameters NA and NB (describing peak shape angle dependence), and the unit cell parameters a, b, c (while keeping atomic fractional coordinates fixed). The experimental background was modelled with a polynomial of degree 20. No corrections were made for line shift or peak asymmetry or broadening due to crystallite size, lattice strain, or preferred orientation. The Pawley refinement results are shown in Figure 1 of the manuscript.

### 2.3.Surface area and porosity analyses

Surface areas were calculated from the experimental gas sorption isotherms with the Brunauer– Emmett–Teller (BET) method. Results are shown on the sorption isotherms.
Pore size distribution (PSD) was modeled from the experimental gas sorption isotherms using the Quantachrome ASiQwin program (version 4.0) with the DFT method “carbons (cylindrical/sphere pores QSDFT adsorption branch)” that gave the best fit for the data. Note that several other QSDFT methods (Quenched Solid Density Functional Theory) led to similar results.

### 2.4. Binding energies calculations

For $AuCl_4^-$ binding, crystalline COF structures were modelled. COF structures and unit cells were first optimized using molecular mechanics with the Forcite module of BIOVIA Materials Studio 2017 (17.1.0.48) (Dassault Systèmes, San Diego, 2017) using Ultra Fine parameters and the Universal Force Field (UFF) imposing the PBAN space group for Tfpy-PDA and Tfpy-PDA-S COFs, and P3 space group for TTT-TAPB and TTT-TAPB-S COFs. These starting structures were further optimized using DFT with the Dmol3 module of BIOVIA Materials Studio 2017 (17.1.0.48) and the following parameters: Generalized Gradient Approximation (GGA)-PW91 functional using the OBS method for DFT-D correction; Medium quality; convergence criteria: Energy 2.0e-5 Ha, Max force 0.004 Ha/Å, Max displacement 0.005 Å; Max iteration 100; Max step size 0.3 Å; no cell optimization; SCF tolerance 1.0e-5; Hexadecapolar expansion; Smearing of 0.01 Ha; k-points: medium quality. Symmetry was applied for

base COFs with their respective space groups (PBAN and P3). Structures were converted to P1 space group to introduce a single $AuCl_4^-$ ion per unit cell at different locations followed by geometry optimization in Dmol3 following the above parameters.
Free $AuCl_4^-$ geometry was optimized with Dmol3 using Fine quality parameters and without smearing.

Relative binding energies are defined as $E_{[COF\text{-}AuCl4-]} - E_{COF} - E_{AuCl4-}$.
For $AuCl_3$ binding, model compounds were generated containing all types of nitrogen and sulfur binding sites in the 4 COFs reported herein: (i) a pyrene core and (ii) a [1,2,4]-triazolo-[1,3,5]-triazine core, each possessing an imine and a thiazole moiety. These model compound structures and their complexes with $AuCl_3$ on different binding sites were optimized by DFT at the ωB97xD/def2-SV(P) level of theory in water using the Polarizable Continuum Model with the Gaussian16 program (G16RevC.02).[1]
Relative binding energies are defined as $E_{[model\text{-}AuCl3]} - E_{model} - E_{AuCl4^-} + E_{Cl^-}$.
Binding modes and energies are shown in Figure S46–S51.

## 3. Synthesis of organic linkers and COFs

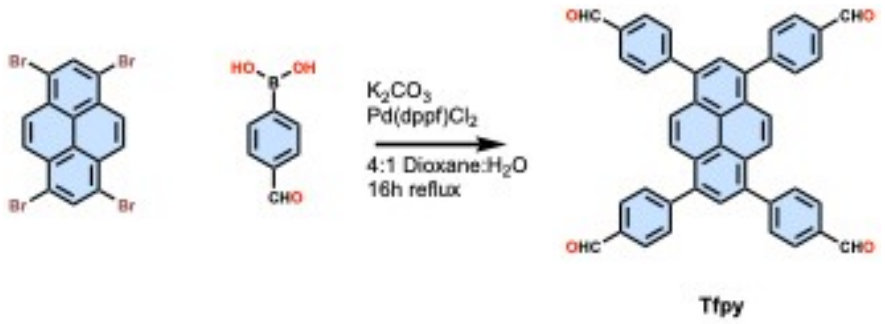


*Figure S1: Synthesis of 1,3,6,8-Tetrakis(4-formylphenyl)pyrene (TFPy)*

**1,3,6,8-Tetrakis(4-formylphenyl)pyrene (Tfpy)**

1,3,6,8-tetrabromopyrene (371 mg, 0.72 mmol, 1.0 eq.) and 4-formylphenylboronic acid (480 mg, 3.20 mmol, 4.8 eq.), 8 mL 1,4-dioxane and 2 mL $H_2O$ were added to a 100 mL 2-necked round bottom flask. The mixture was refluxed under argon using a heating mantle for 30 minutes to degas the reaction mixture. Under an argon stream, $K_2CO_3$ (547 mg, 3.66 mmol, 5.5 eq.) and $Pd(dppf)Cl_2$ (26 mg, 0.036 mmol, 5 mol%) were added in one portion. Reflux under argon was continued for 16h. After cooling to room temperature, 20 mL $H_2O$ was added to the mixture. The precipitate was collected by filtration and washed with $H_2O$ and MeOH. The resulting powder was dried under vacuum (404 mg, 0.65 mmol, 91% yield). This procedure was adapted from literature.[2]

$^1$H NMR (300 MHz, $CDCl_3$, 298 K): δ (ppm) = 10.17 (s, 4H), 8.18 (s, 4H), 8.10 (d, 8H), 8.04 (s, 2H), 7.86 (d, 8H).

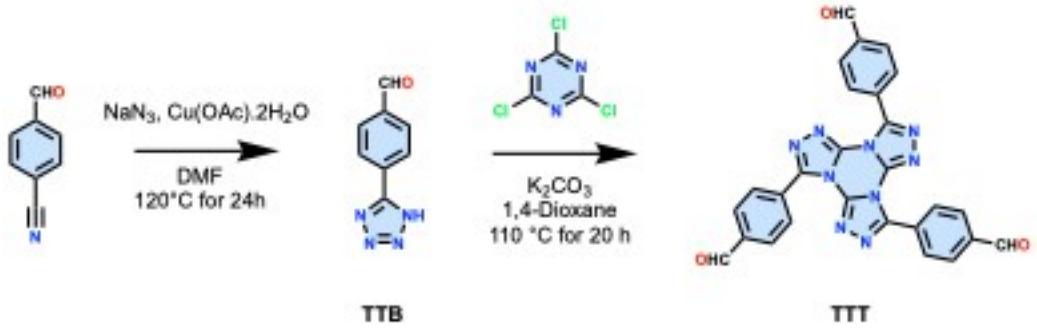


Figure S2: Synthesis of 4,4',4''- (tris((1,2,4)triazolo)-(1,3,5)-triazine-tribenzaldehyde (TTT)

**4-(1H-tetrazol-5-yl)benzaldehyde (TTB)**

1.31 g 4-formylbenzonitrile (10 mmol), 780 mg sodium azide (12 mmol), and 200 mg $Cu(OAc)_2.H_2O$ were added to a 20 mL Schlenk tube. 10 mL DMF was added, and the mixture was sparged with argon for 15 minutes. The headspace of the Schlenk tube was then flushed with argon, and the tube was closed, then heated at 120°C for 24 hours. After cooling to room temperature, the con- tents of the Schlenk tube were transferred to a 100 mL beaker, and 20 mL of a 5M HCl solution was added. This mixture was stirred for 30 minutes at room temperature. The obtained white precipitate was washed with water and methanol, then dried under vacuum for 16 hours (1.695 g, 95% yield). The synthesis was adapted from literature.[3]

$^1$H NMR (300 MHz, DMSO-$d_6$, 298 K): δ (ppm) = 10.10 (s, 1H), 8.26 (d, 2H), 8.14 (d, 2H).

**4,4',4''- (tris((1,2,4)triazolo)-(1,3,5)-triazine-tribenzaldehyde (TTT)**

870 mg 4-(1H-tetrazol-5-yl)benzaldehyde, 275 mg cyanuric chloride and 2.78 g $K_2CO_3$ were added to 40 mL of dry dioxane. The mixture was sparged with argon for 15 minutes, then refluxed at 110 °C under argon for 20 hours. The dioxane solvent was removed under reduced pressure and methanol was added to the residue. The off-white precipitate was filtered and washed with water, methanol, then dried under vacuum for 16 hours (0.125 g, 26% yield). Synthesis was adjusted from literature.[3]

$^1$H NMR (300 MHz, DMSO-$d_6$, 298 K): δ (ppm) = 10.18 (s, 93), 8.25 (d, 6H), 8.20 (d, 6H).

**Synthesis of Tfpy-PDA COF**

The procedure was adjusted from literature.[2] TFPPy (360 mg, 0.501 mmol, 1 eq.) and p-phenylenediamine (110 mg, 1.02 mmol, 2 eq.) were added to a 40 mL glass vial equipped with a stirring bar (with a length of 1 cm). To this vial 19.4 mL of a mixture containing 67 V% n-butanol, 23 V% glacial acetic acid, and 10 V% $H_2O$. Finally, the vial was closed with a screwcap and the resulting solution was bubbled for 15 min with Ar through a needle. The mixture was stirred at 70°C and stirred for 16 hours. After cooling to room temperature, the obtained COF was filtered over a nylon filter of 0.45µm pore diameter, washed with 10 mL $H_2O$, 2x10 mL methanol, then 2x10 mL acetone. The resulting powder was dried under vacuum at 90°C for 16h (0.402 g, 93% yield).

**Synthesis Tfpy-PDA-S COF**

In a glass ampule were added 20 mg of Tfpy-PDA COF and 200 mg of elemental sulfur (a 1:10 mass ratio). The ampule was evacuated under vacuum for 15 min and flame-sealed. The ampule was heated to 150 °C ( at 5 °C min$^{-1}$ heating rate) for 3 hours, then the temperature was raised to 310 °C (at 0.89 °C min$^{-1}$ heating rate) and kept for 6 hours at this temperature. After cooling to room temperature, the residue was washed overnight with 50 mL of a 3/2 volume ratio solution of ortho-dichlorobenzene/chlorobenzene at 100 °C to remove the residual sulfur. The solid was collected by filtration and washed with water, methanol, and acetone. The resulting dark yellow powder was dried at 90 °C under vacuum for 16 hours. (19.1 mg, 88% yield)

**Synthesis TTT-TAPB COF**

31 mg TTT (0.06 mmol) and 21 mg TAPB (0.09 mmol) were added to a 4 mL glass vial containing an oblong teflon stirring bar with a length of 1 cm. 1.5 mL of a solution consisting of 1 mL n-butanol, 0.150 mL water and 0.350 mL glacial acetic acid was added. The vial was closed with a plastic screwcap, and stirred at 250 rpm at 70 °C for 16 hours in an aluminium heating block. After cooling to room temperature, the solid from the resulting yellow slurry was collected by filtration over a nylon filter of 0.45 µm pore diameter, washed with 10 mL $H_2O$, 10 mL DMF, 10 mL acetone, then 10 mL methanol. The powder was soaked in the solvent for 10 minutes each washing step. The resulting bright-yellow powder was dried at 90°C under vacuum for 16 hours (36 mg, 94% yield).

**Synthesis TTT-TAPB-S COF**

For the post-synthetic modification of the imine linkage to the thiazole linkage, 20 mg of TAPB-TTT was thoroughly ground with 200 mg of elemental sulfur (a 1:10 mass ratio) for 5 minutes in an agate pestle and mortar. The resulting mixture was transferred to a glass ampoule, evacuated to 0.40 mbar for 5 minutes, and flame-sealed under vacuum. The ampoule was heated in a muffle furnace. The temperature was first increased to 155 °C over a period of two hours, then held at 155 °C for 3 hours. Then, the tem- perature was increased to 320 °C over 3 hours and held at this temperature for 5 hours, before cooling down to room temperature. The ampoule was opened, and the obtained brown monolith was soaked in 20 mL of chlorobenzene/o-dichlorobenzene in a 2:3 volume ratio at 120 °C while stirring

overnight. The material was filtered over a nylon filter of 0.45 µm pore diameter, washed with methanol and acetone, and dried under vacuum for 16 hours. (19.3 mg, 85%)

# 4. Characterization of COFs

## 4.1 Stacking models

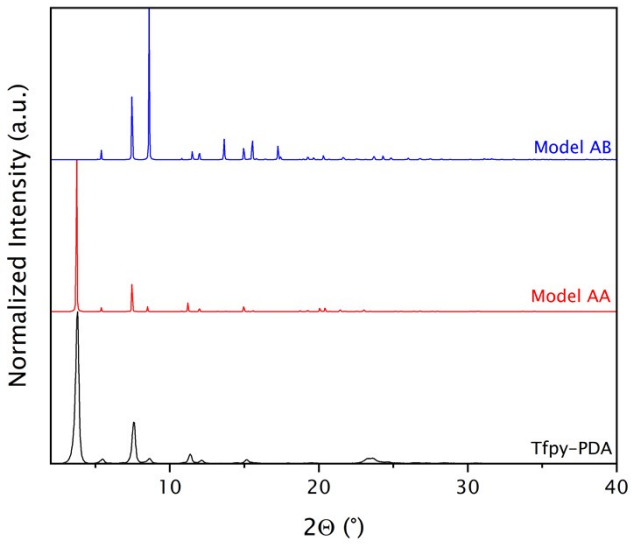


*Figure S3: AB and AA stacking models of Tfpy-PDA COF*

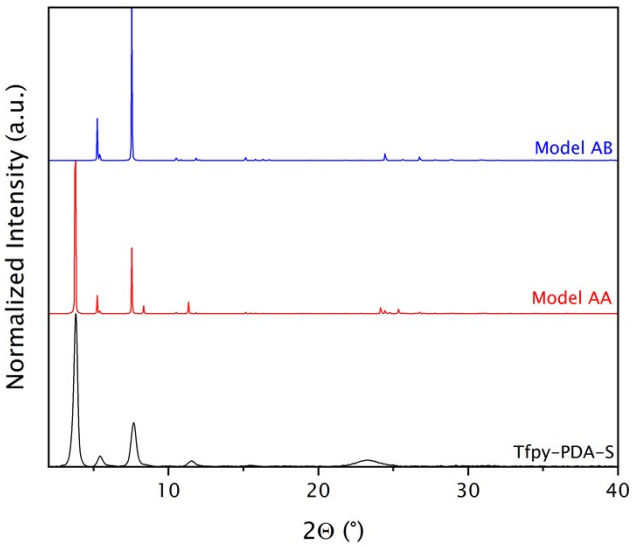


*Figure S4: AB and AA stacking models of Tfpy-PDA-S COF*

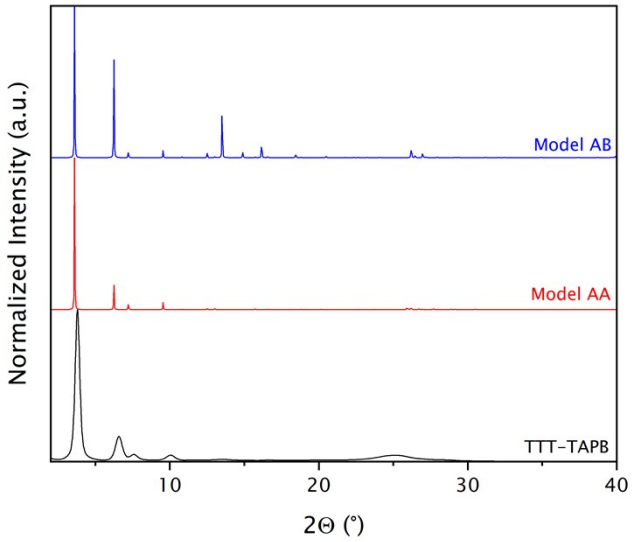


*Figure S5: AB and AA stacking models of TTT-TAPB COF*

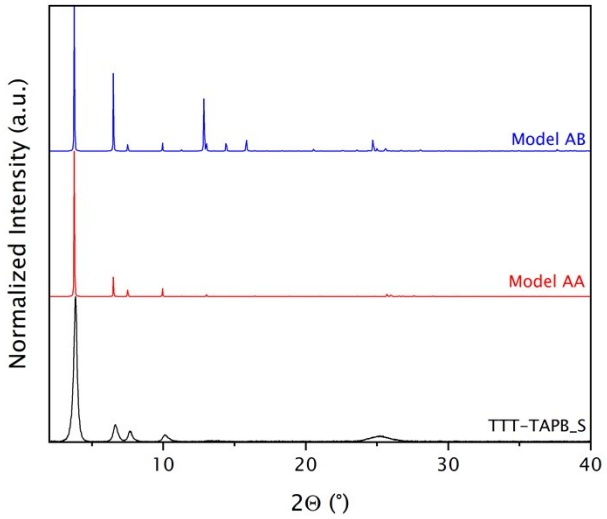


*Figure S6: AB and AA stacking models of TTT-TAPB-S COF*

### 4.2 Atomic positions

**Table S1: Atomic positions Tfpy-PDA**

Crystal system: Orthorombic
Space group: Cmm2 (35)
a 34.2503 Å b 32.7542 Å c 4.4228 Å
α 90.0° β 90.0° γ 90.0°
V = 4961.68 Å³

| Label | $x_{frac}$ | $y_{frac}$ | $z_{frac}$ |
|---|---|---|---|
| C1 | 0.46475 | 0.95818 | 0.98552 |
| C2 | 0.43015 | 0.0205 | 0.98194 |
| C3 | 0.46504 | 0.0835 | 0.98747 |
| C4 | 0.42944 | 0.10696 | 1.00384 |
| C5 | 0.40873 | 0.10725 | 1.18652 |
| C6 | 0.3756 | 0.13014 | 1.20495 |
| C7 | 0.36271 | 0.1531 | 1.04111 |
| C8 | 0.38356 | 0.15275 | 0.85787 |
| C9 | 0.41681 | 0.12993 | 0.83986 |
| C10 | 0.32785 | 0.17736 | 1.06604 |
| C11 | 0.78197 | 0.27558 | 0.9261 |
| C12 | 0.76593 | 0.26254 | 0.74332 |
| C13 | 0.73408 | 0.23748 | 1.11032 |
| H1 | 0.40268 | 0.03535 | 0.97766 |
| H2 | 0.4184 | 0.08991 | 1.31497 |
| H3 | 0.36013 | 0.13006 | 1.34778 |
| H4 | 0.37432 | 0.1702 | 0.72904 |
| H5 | 0.43267 | 0.13009 | 0.69823 |
| H6 | 0.31298 | 0.17617 | 1.2102 |
| H7 | 0.77813 | 0.27213 | 0.60084 |
| H8 | 0.722 | 0.22895 | 1.25433 |
| N1 | 0.31496 | 0.19898 | 0.91791 |
| C15 | 0.5 | 0.10372 | 0.98552 |
| C14 | 0.5 | 0.97907 | 0.9848 |
| H9 | 0.5 | 0.13568 | 0.99035 |

**Table S2: Atomic positions Tfpy-PDA-S**

Crystal system: Orthorombic
Space group: Cmm2 (35)
a 32.5961 Å b 33.6194 Å c 3.6809 Å
α 90.0° β 90.0° γ 90.0°
V = 4033.76 Å³

| Label | $x_{frac}$ | $y_{frac}$ | $z_{frac}$ |
|---|---|---|---|
| C1 | 0.46392 | 0.95768 | 0.93458 |
| C2 | 0.42959 | 0.02051 | 0.86743 |
| C3 | 0.46374 | 0.08622 | 0.97673 |
| C4 | 0.42704 | 0.1107 | 0.99003 |
| C5 | 0.39288 | 0.09775 | 1.16736 |
| C6 | 0.35874 | 0.12067 | 1.17106 |
| C7 | 0.35858 | 0.15821 | 1.0153 |
| C8 | 0.39307 | 0.17222 | 0.85289 |
| C9 | 0.42661 | 0.14851 | 0.8345 |
| C10 | 0.32282 | 0.18288 | 1.02299 |
| C11 | 0.78881 | 0.262 | 1.02203 |
| C12 | 0.75898 | 0.28969 | 1.02549 |
| H13 | 0.40192 | 0.03465 | 0.81198 |
| H14 | 0.39251 | 0.07017 | 1.30919 |
| H15 | 0.33294 | 0.10954 | 1.30803 |
| H16 | 0.39369 | 0.201 | 0.7285 |
| H17 | 0.45202 | 0.15964 | 0.69155 |
| S18 | 0.77592 | 0.33675 | 1.0302 |
| N19 | 0.32502 | 0.22258 | 1.01815 |
| C20 | 0.21933 | 0.77839 | 1.02355 |
| H21 | 0.19592 | 0.80001 | 1.0234 |
| C22 | 0.5 | 0.10553 | 1.01326 |
| C23 | 0.5 | 0.97804 | 0.94359 |
| H24 | 0.5 | 0.13667 | 1.0742 |

**Table S3: Atomic positions TTT-TAPB**

Crystal system: Hexagonal
Space group: P-6 (174)
a 26.8776 Å b 26.8776 Å c 3.2949 Å
α 90.0° β 90.0° γ 120.0°
V = 2061.36 Å³

| Label | $x_{frac}$ | $y_{frac}$ | $z_{frac}$ |
|---|---|---|---|
| N1 | 0.388 | 0.70457 | 0 |
| C2 | 0.35014 | 0.72055 | 0 |
| C3 | 0.43663 | 0.75313 | 0 |
| N4 | 0.42608 | 0.79476 | 0 |
| N5 | 0.37281 | 0.77456 | 0 |
| C6 | 0.49571 | 0.7668 | 0 |
| C7 | 0.51506 | 0.72953 | 0 |
| C8 | 0.57088 | 0.74723 | 0 |
| C9 | 0.60958 | 0.80276 | 0 |
| C10 | 0.59153 | 0.8406 | 0 |
| C11 | 0.53582 | 0.82294 | 0 |
| C12 | 0.66821 | 0.8202 | 0 |
| C13 | 0.97488 | 0.03147 | 0 |
| C14 | 0.94173 | 0.97413 | 0 |
| C15 | 0.87958 | 0.94655 | 0 |
| C16 | 0.85227 | 0.97712 | 0 |
| C17 | 0.79542 | 0.95168 | 0 |
| C18 | 0.76321 | 0.89505 | 0 |
| C19 | 0.789 | 0.86373 | 0 |
| C20 | 0.84588 | 0.88889 | 0 |
| N21 | 0.70491 | 0.8717 | 0 |
| H22 | 0.48973 | 0.68684 | 0 |
| H23 | 0.58387 | 0.71713 | 0 |
| H24 | 0.62038 | 0.88399 | 0 |
| H25 | 0.52456 | 0.85427 | 0 |
| H26 | 0.67956 | 0.78902 | 0 |
| H27 | 0.95573 | 0.05543 | 0 |
| H28 | 0.87315 | 1.02092 | 0 |
| H29 | 0.77619 | 0.97652 | 0 |
| H30 | 0.766 | 0.81972 | 0 |
| H31 | 0.86169 | 0.8614 | 0 |

**Table S4: Atomic positions TTT-TAPB-S**

Crystal system: Hexagonal
Space group: P-6 (174)
a 26.5922 Å b 26.5922 Å c 3.2948 Å
α 90.0° β 90.0° γ 120.0°
V = 2017.75 Å³

| Label | $x_{frac}$ | $y_{frac}$ | $z_{frac}$ |
|---|---|---|---|
| N1 | 0.3873 | 0.71289 | 0 |
| C2 | 0.34128 | 0.71992 | 0 |
| C3 | 0.43228 | 0.76774 | 0 |
| N4 | 0.41185 | 0.80406 | 0 |
| N5 | 0.35584 | 0.77449 | 0 |
| C6 | 0.49618 | 0.79246 | 0 |
| C7 | 0.52564 | 0.762 | 0 |
| C8 | 0.58504 | 0.78973 | 0 |
| C9 | 0.61761 | 0.84915 | 0 |
| C10 | 0.58926 | 0.88023 | 0 |
| C11 | 0.52998 | 0.85253 | 0 |
| C12 | 0.68064 | 0.8789 | 0 |
| C13 | 0.98861 | 0.04451 | 0 |
| C14 | 0.94245 | 0.98828 | 0 |
| C15 | 0.88108 | 0.97576 | 0 |
| C16 | 0.86754 | 1.02032 | 0 |
| C17 | 0.81115 | 1.00875 | 0 |
| C18 | 0.76753 | 0.95266 | 0 |
| C19 | 0.7787 | 0.90891 | 0 |
| C20 | 0.83429 | 0.91897 | 0 |
| N21 | 0.71219 | 0.93625 | 0 |
| H22 | 0.50574 | 0.71736 | 0 |
| H23 | 0.60524 | 0.76404 | 0 |
| H24 | 0.6128 | 0.92625 | 0 |
| H25 | 0.51087 | 0.8792 | 0 |
| H27 | 0.97993 | 0.07843 | 0 |
| H28 | 0.89912 | 1.06467 | 0 |
| H29 | 0.80184 | 1.04313 | 0 |
| S30 | 0.71893 | 0.84378 | 0 |
| H31 | 0.8388 | 0.88187 | 0 |

### 4.3 BET plots & pore size distributions

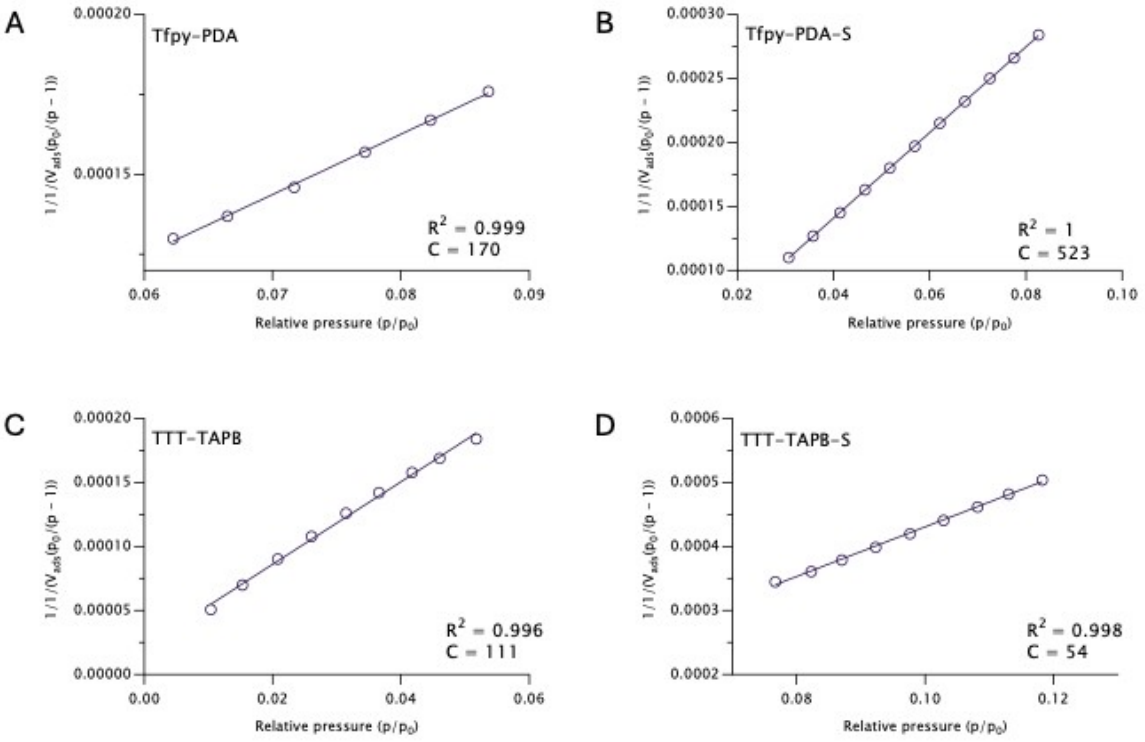


*Figure S7: BET plots of A) Tfpy-PDA, B) Tfpy-PDA-S, C) TTT-TAPB, D) TTT-TAPB-S*

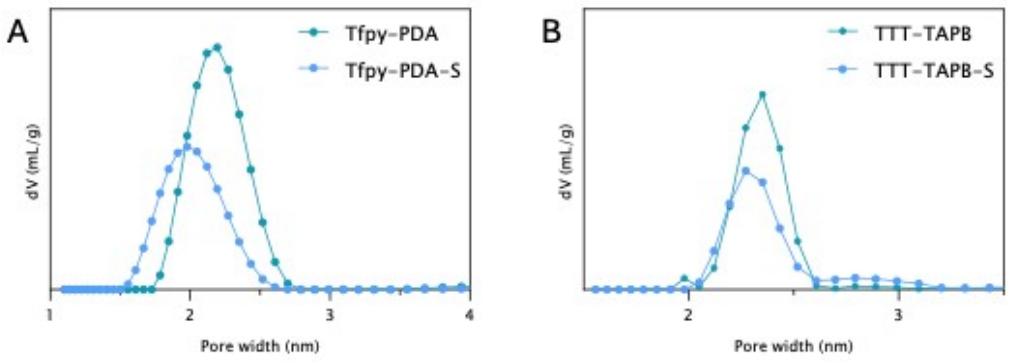


*Figure S8: Pore size distribution of A) Tfpy-PDA(-S) and B) TTT-TAPB(-S).*

### 4.4 Mott-Shottky Analyses

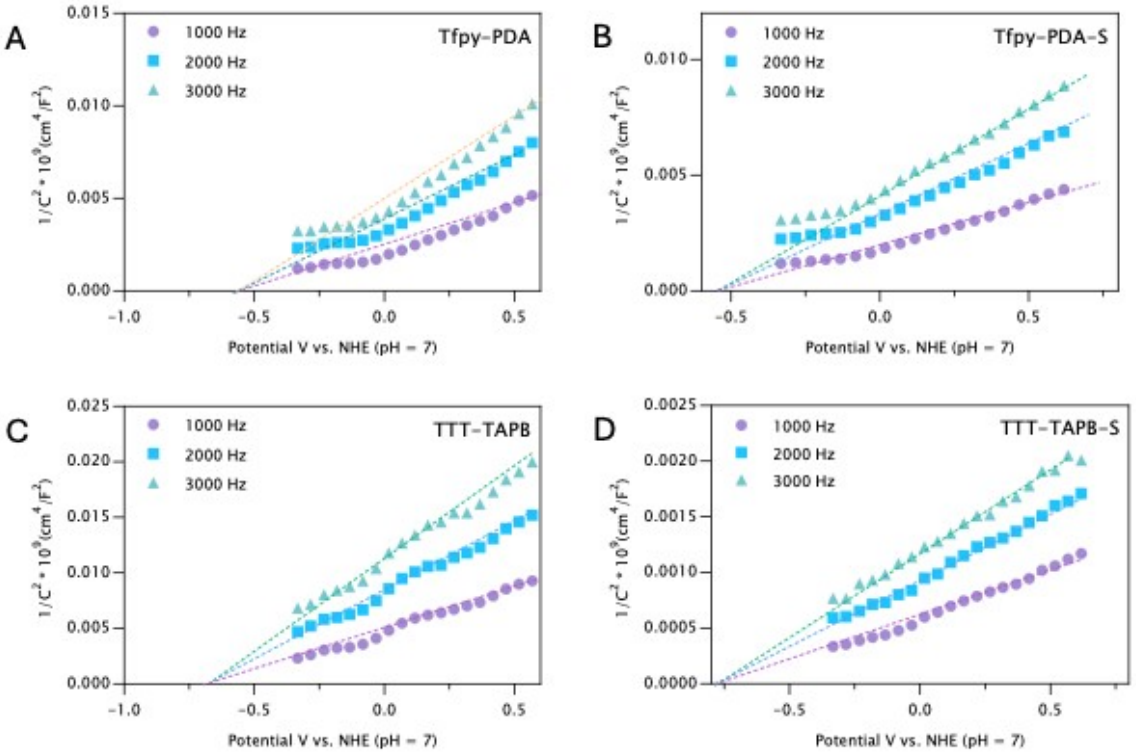


*Figure S9: Mott-Shottky curves (vs. NHE, pH = 7) of A) Tfpy-PDA, B) Tfpy-PDA-S, C) TTT-TAPB, D) TTT-TAPB-S.*

### 4.5 Solid-state ultraviolet spectroscopy (UV-Vis)

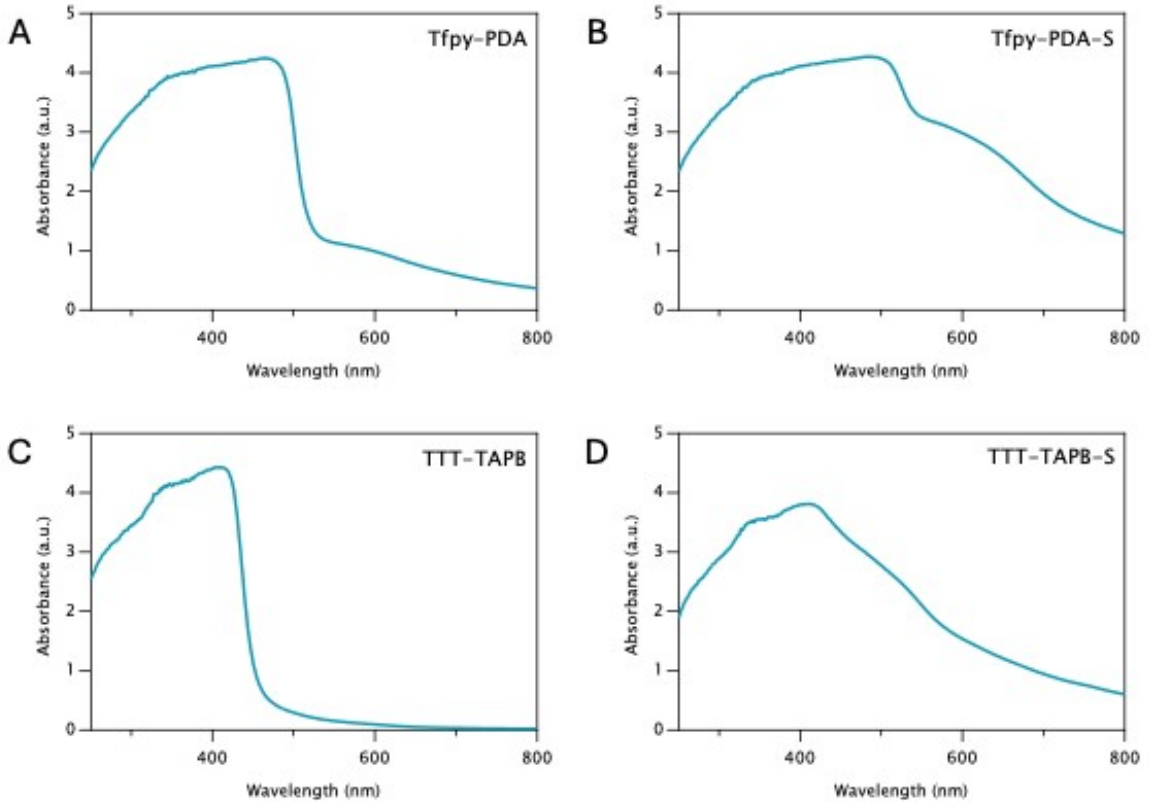


*Figure S10: Solid-state UV-Vis absorption spectra of A) Tfpy-PDA, B) Tfpy-PDA-S, C) TTT-TAPB, D) TTT-TAPB-S.*

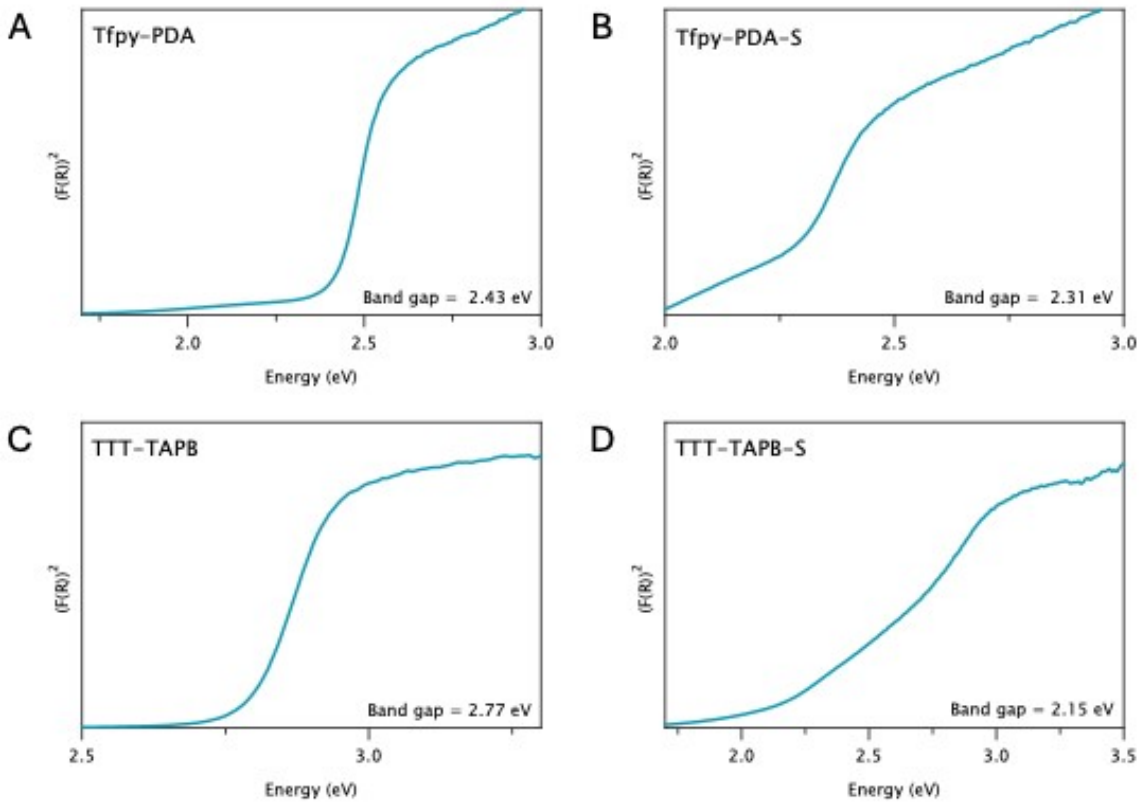


*Figure S11: Tauc plot of A) Tfpy-PDA, B) Tfpy-PDA-S, C) TTT-TAPB, D) TTT-TAPB-S*

### 4.6 Chronoamperometric photocurrent response

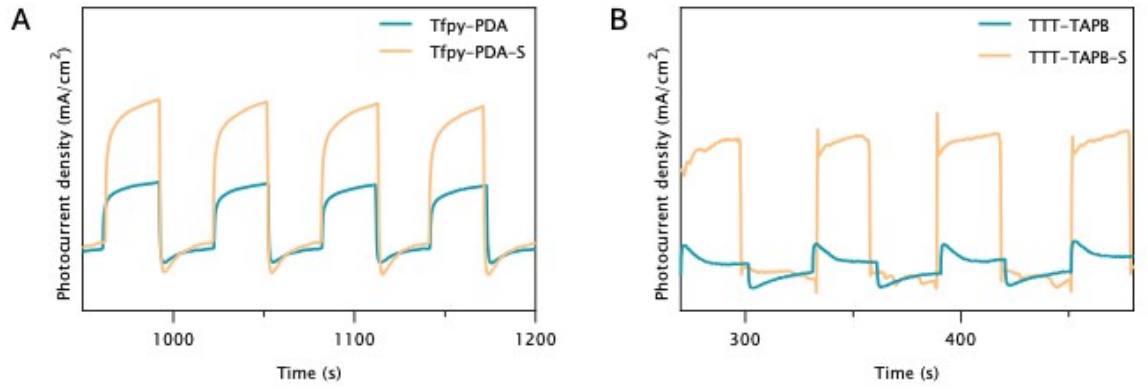


*Figure S12: Photocurrent response curves of A) Tfpy-PDA(-S) and B) TTT-TAPB(-S).*

### 4.7 Thermogravimetrical analysis (TGA)

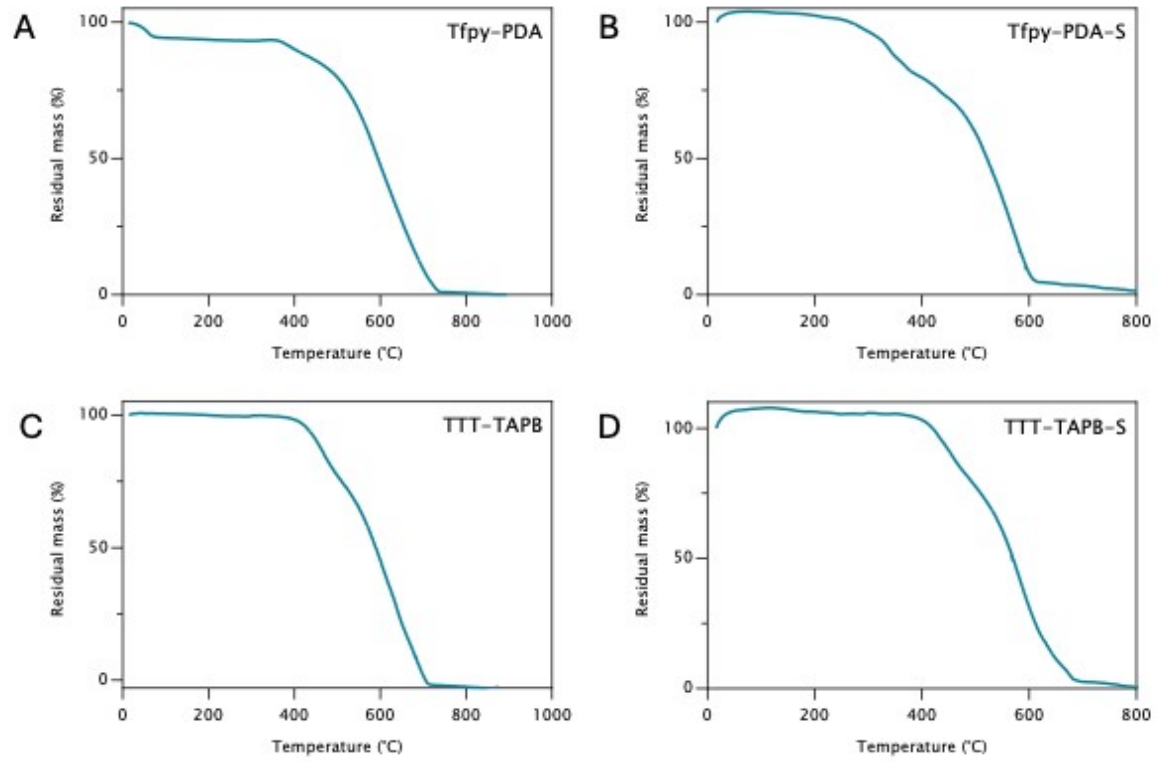


*Figure S13: Thermogravimetrical analysis (TGA) of A) Tfpy-PDA, B) Tfpy-PDA-S, C) TTT-TAPB, D) TTT-TAPB-S.*

## 4.8 Fourrier-Transform Infrared Spectroscopy (FTIR)

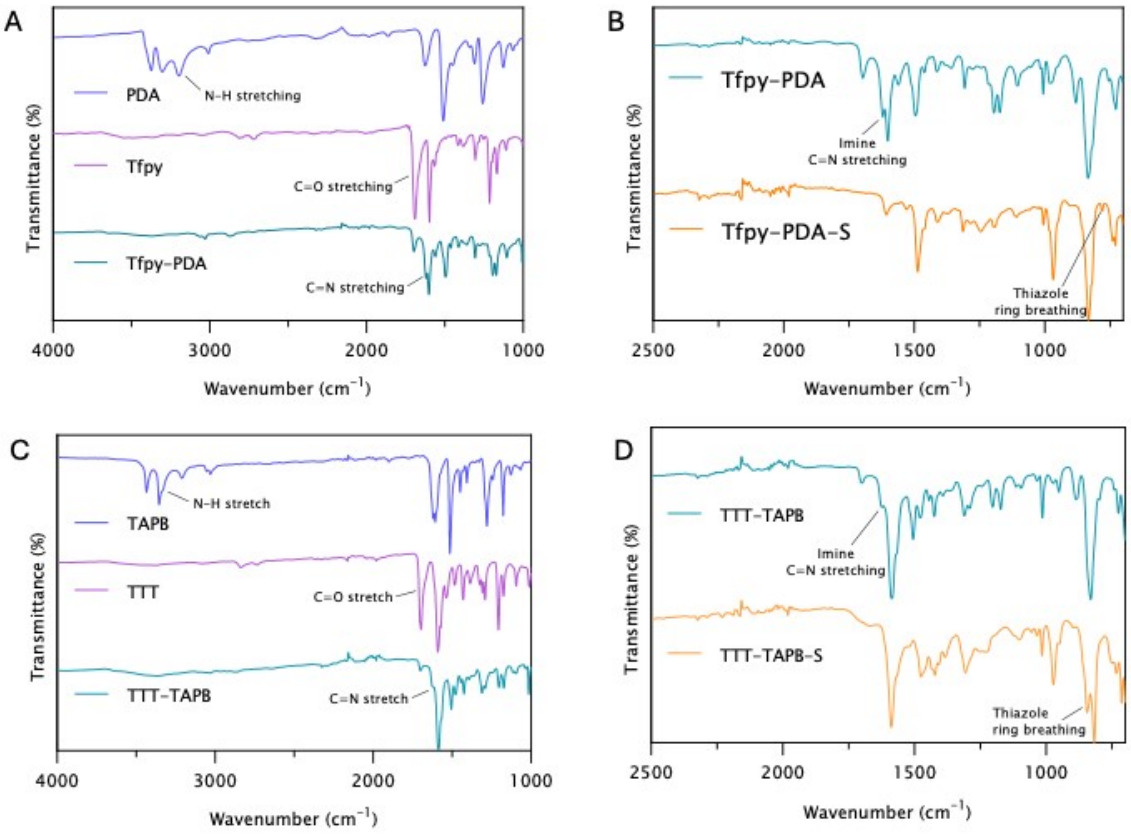


*Figure S14: FTIR spectra of synthesis A) Tfpy-PDA, B) Tfpy-PDA-S, C) TTT-TAPB, D) TTT-TAPB-S.*

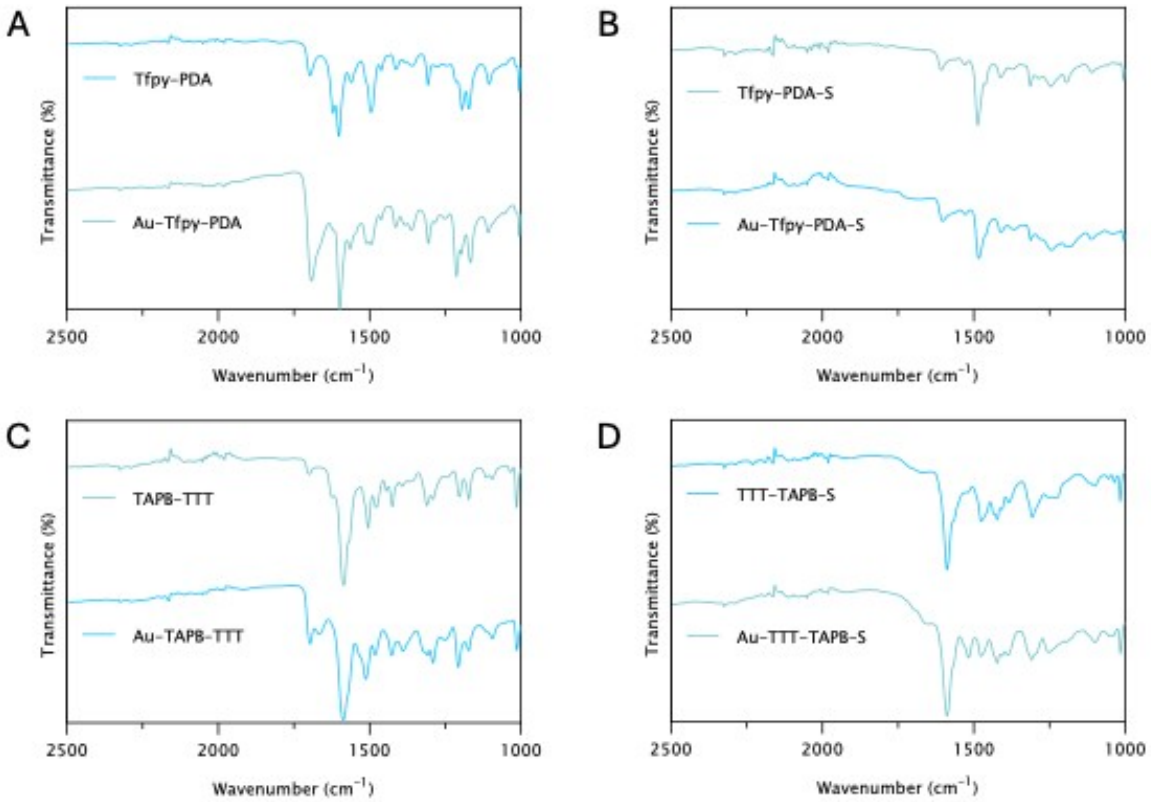


*Figure S15: FTIR spectra overlap of pristine COFs and gold loaded COFs.*

### 4.9 X-Ray Photoelectron Spectroscopy

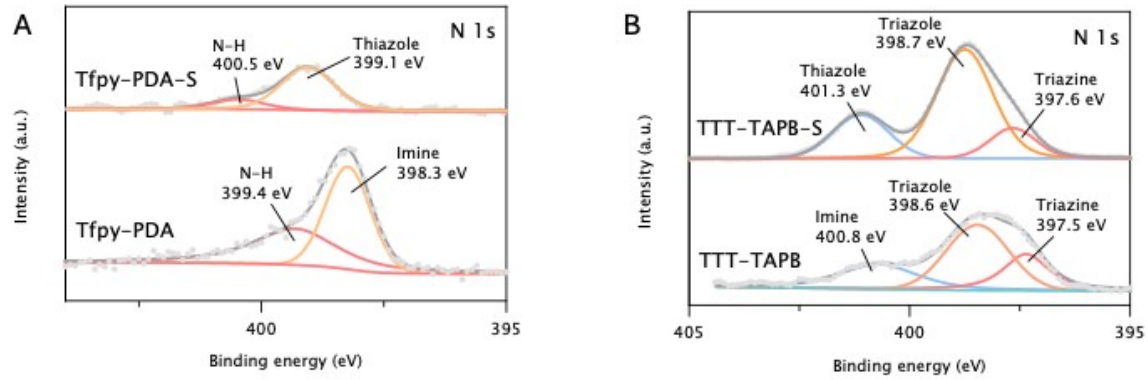


*Figure S16: Nitrogen (N 1s) XPS spectra of A) Tfpy-PDA and Tfpy-PDA-S and B) TTT-TAPB and TTT-TAPB-S.*

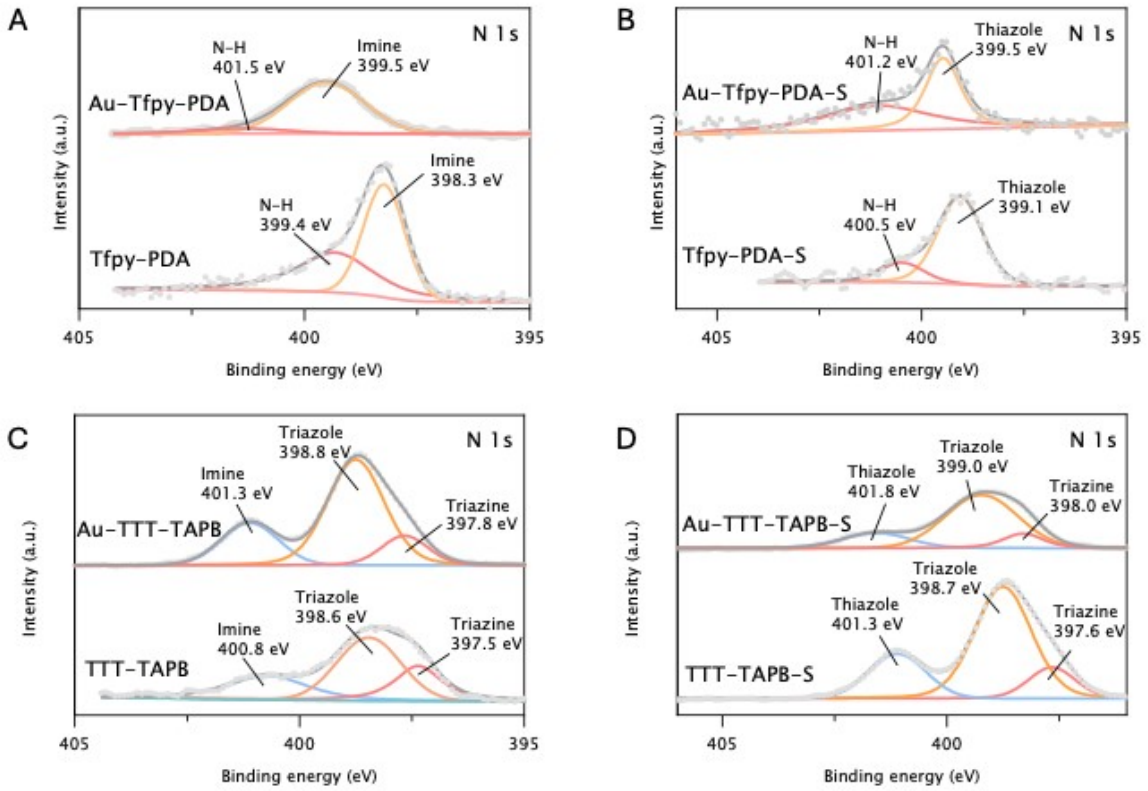


*Figure S17: Nitrogen (N 1s) XPS spectra of A) Tfpy-PDA and Au-Tfpy-PDA, B) Tfpy-PDA-S and Au-Tfpy-PDA-S, C) TTT-TAPB and Au-TTT-TAPB, D) TTT-TAPB-S and Au-TTT-TAPB-S.*

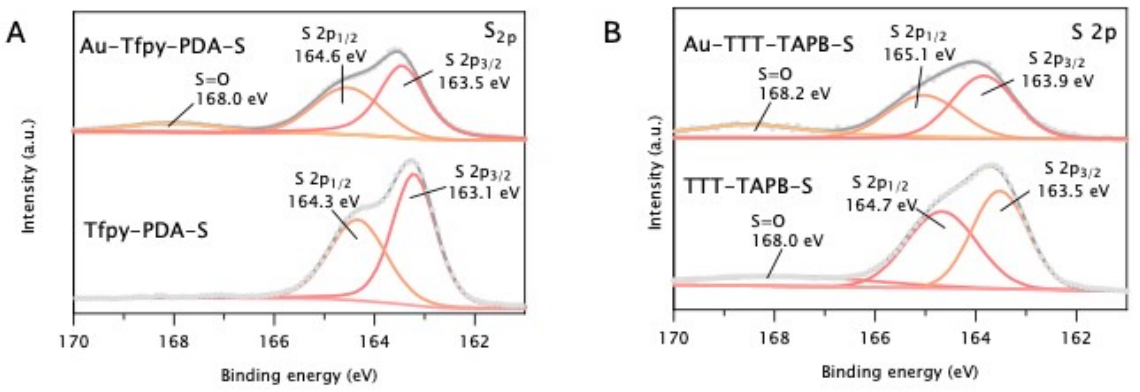


*Figure S18: Sulfur (S 2p) XPS spectra of A) Tfpy-PDA and Au-Tfpy-PDA-S, B) Tfpy-PDA-S and Au-Tfpy-PDA-S.*

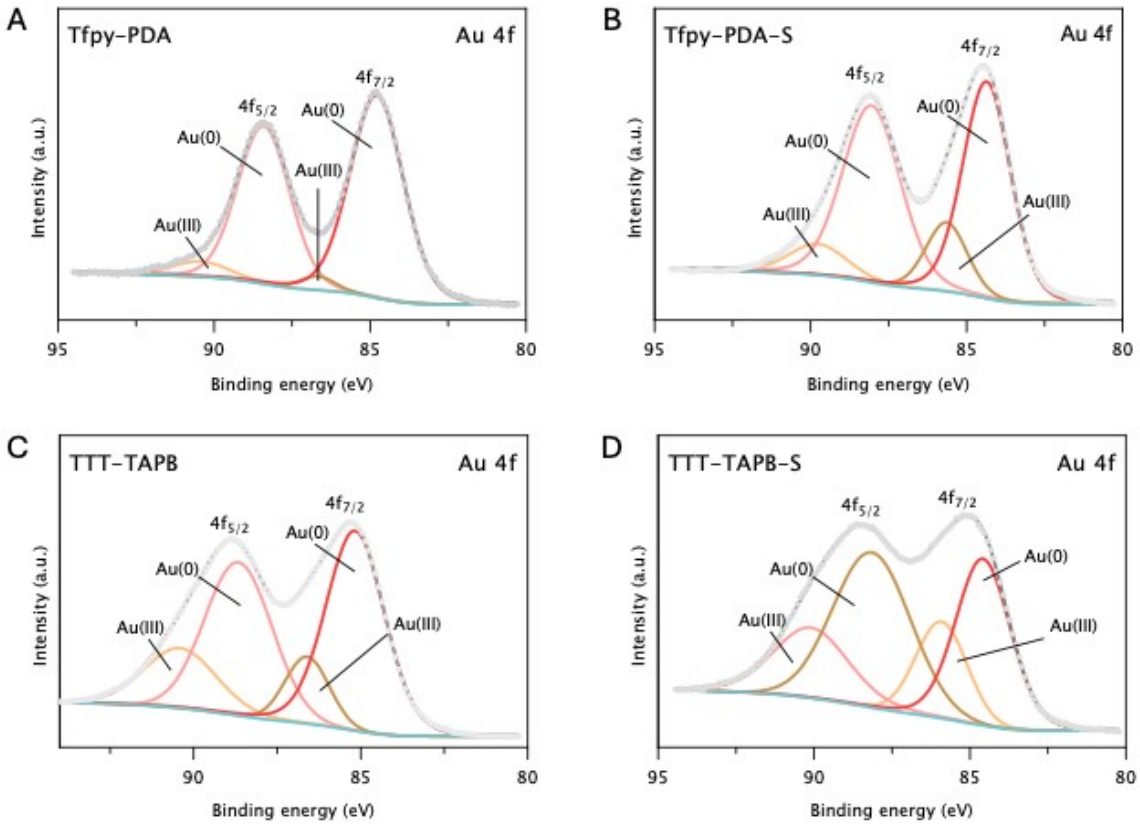


*Figure S19: Gold (Au 4f) XPS spectra after gold adsorption onto A) Tfpy-PDA, B) Tfpy-PDA-S, C) TTT-TAPB, D) TTT-TAPB-S.*

**4.10Zeta potential**

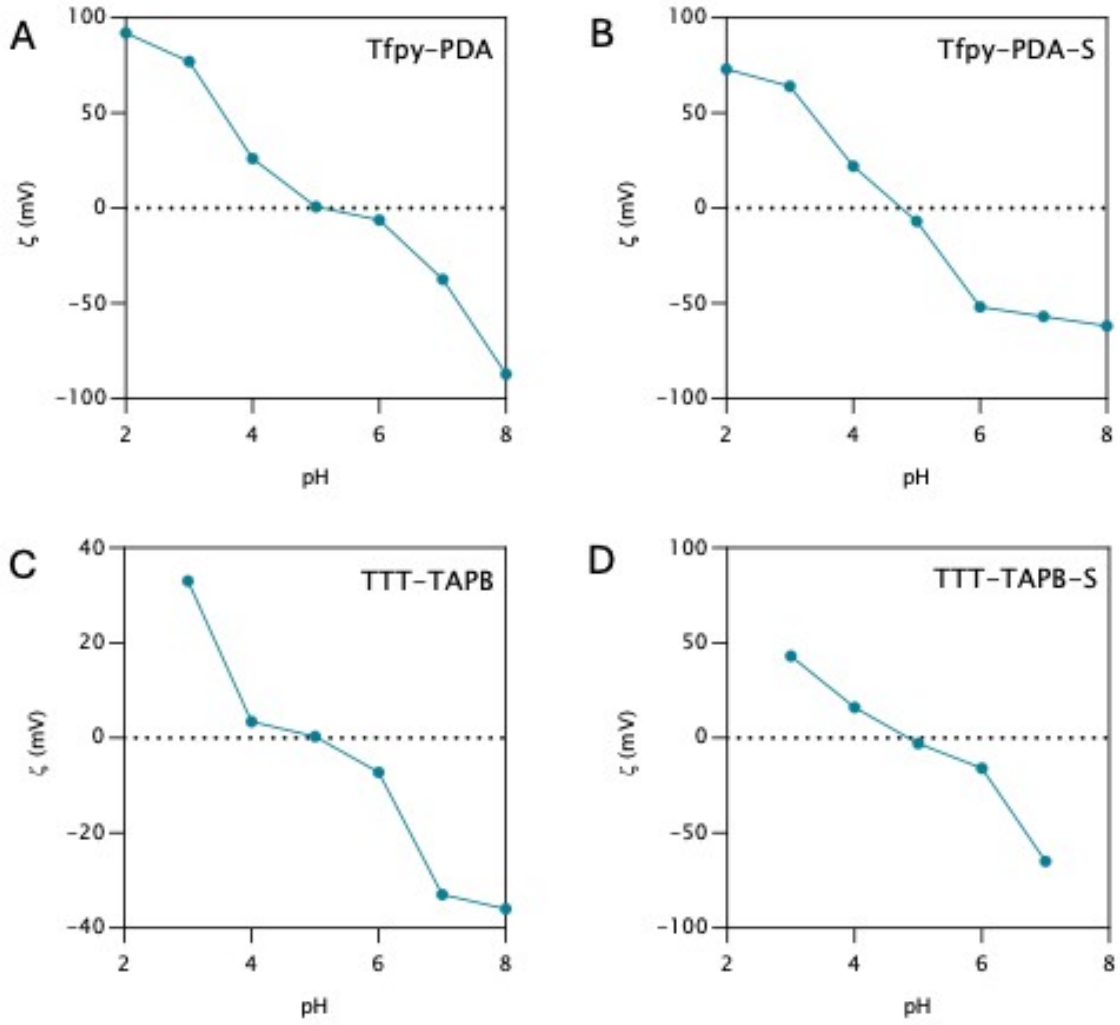


*Figure S20: Zeta potential in function of pH of A) Tfpy-PDA, B) Tfpy-PDA-S, C) TTT-TAPB, D) TTT-TAPB-S.*

### 4.11 Tranmission electron microscopy (TEM)

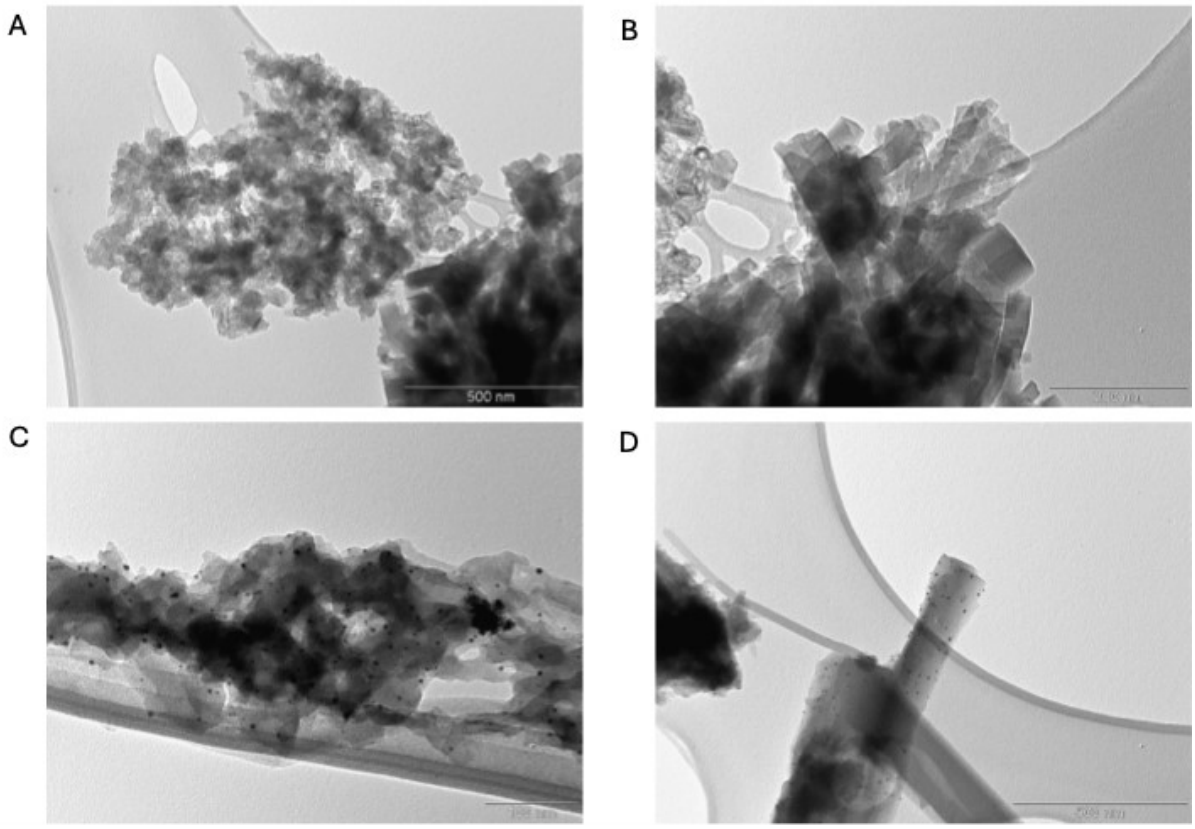


*Figure S21: TEM images of A,B) Tfpy-PDA and C,D) Au-Tfpy-PDA.*

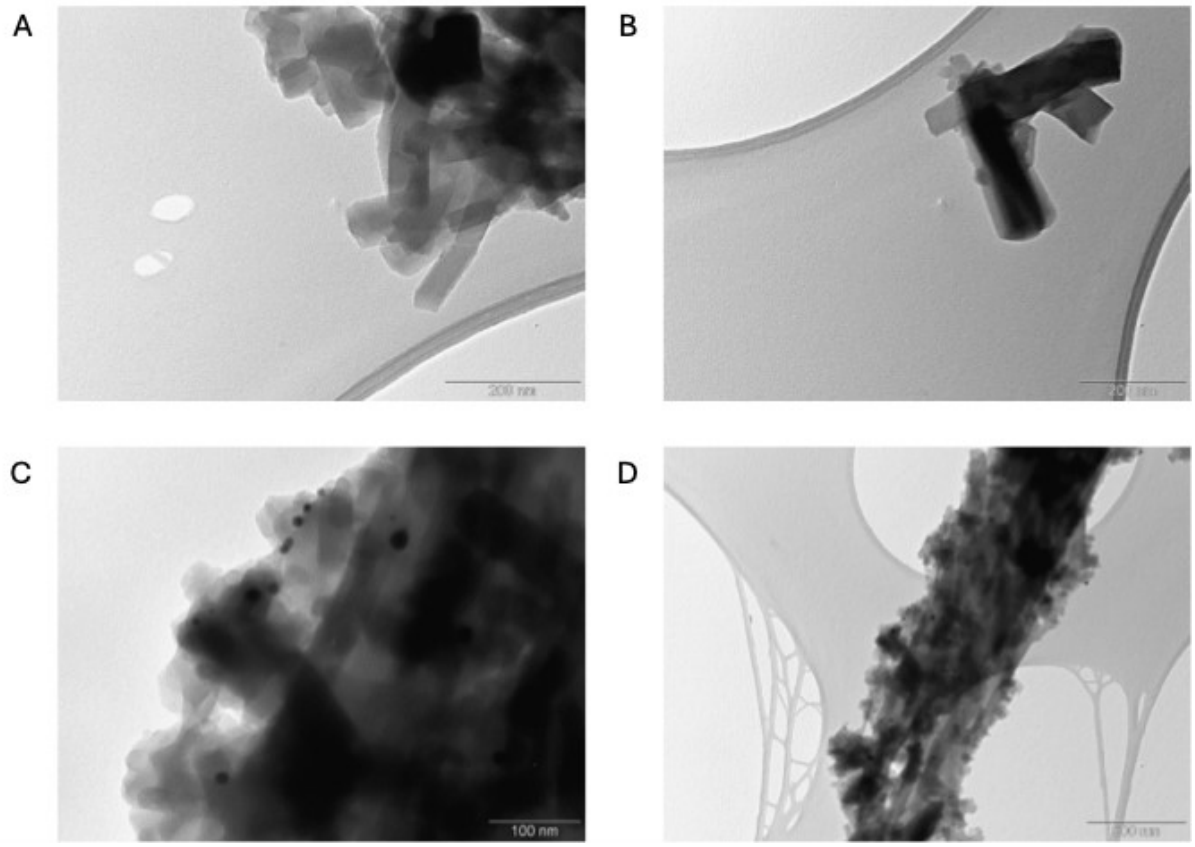


*Figure S22: TEM images of A,B) Tfpy-PDA-S and C,D) Au-Tfpy-PDA-S.*

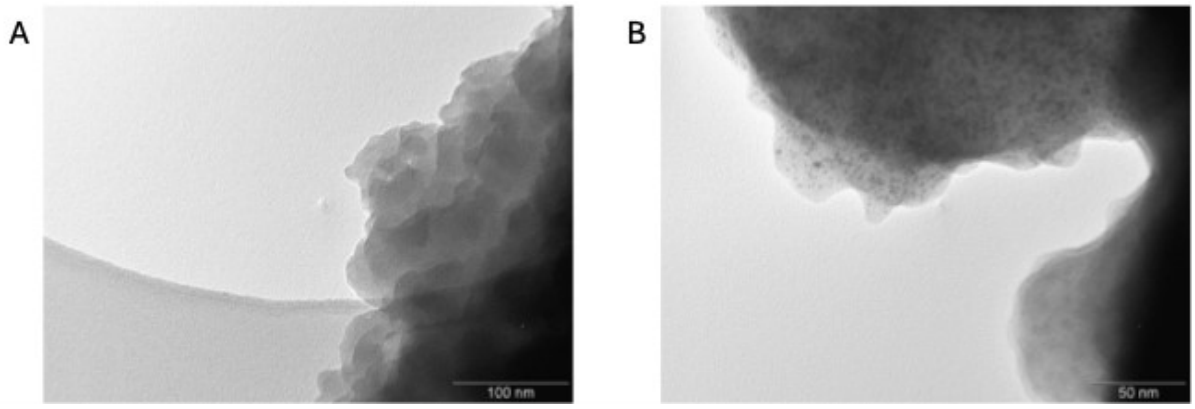


*Figure S23: TEM images of A) TTT-TAPB and B) Au-TTT-TAPB.*

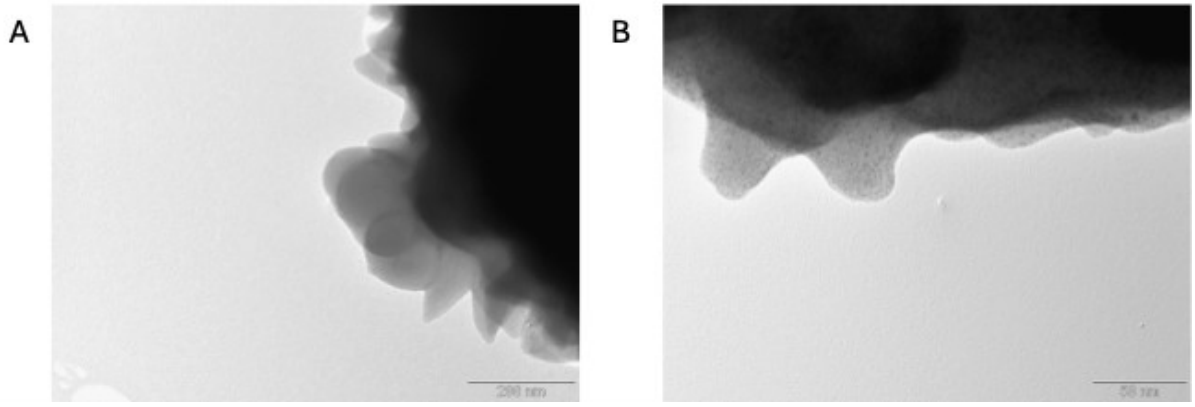


*Figure S24: TEM images of A) TTT-TAPB-S and B) Au-TTT-TAPB-S.*

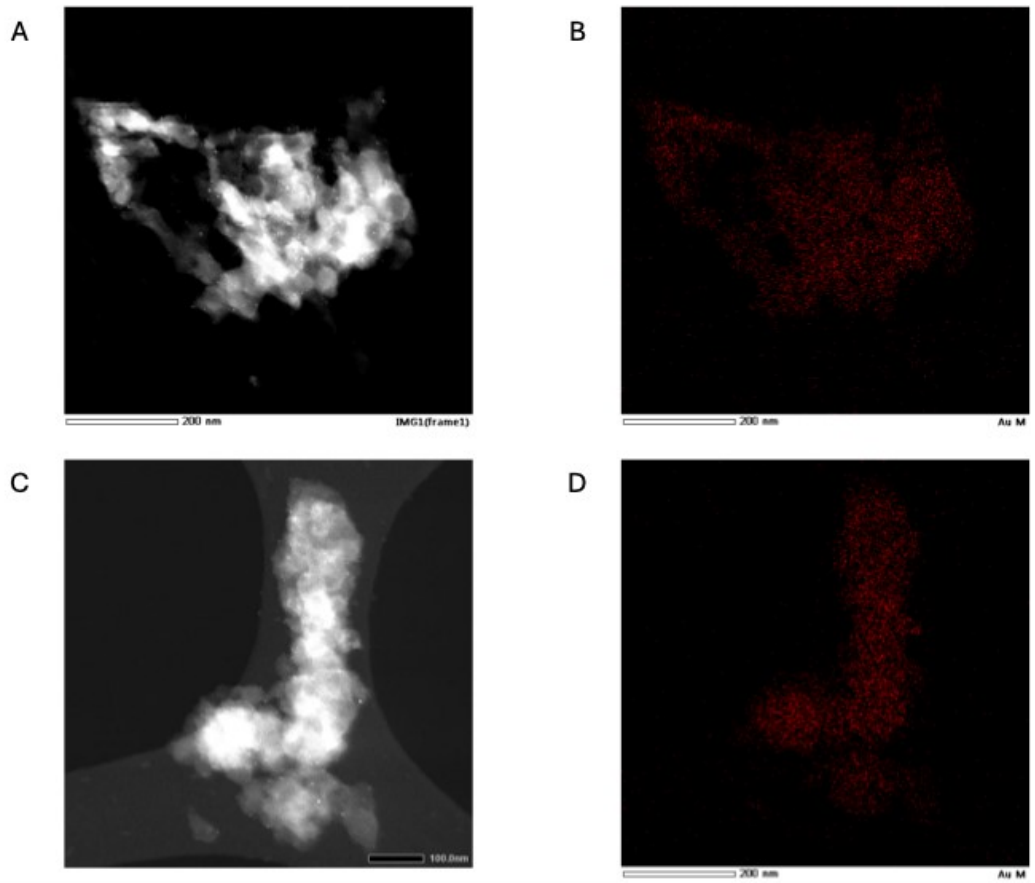


*Figure S25: TEM images and corresponding EDX analyses of* ***(a, b)*** *Au@Tfpy-PDA and* ***(c, d)*** *Au@Tfpy-PDA-S.*

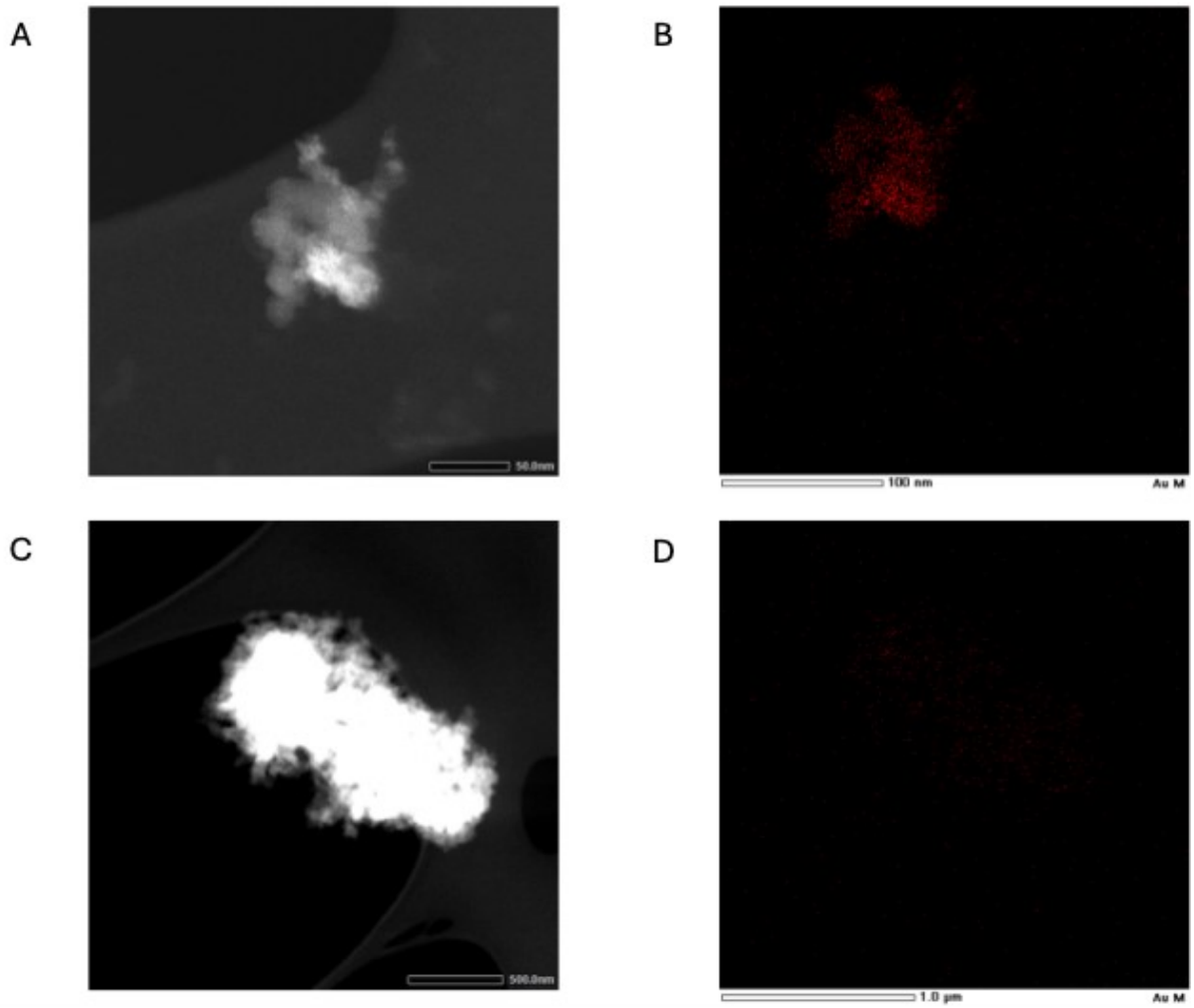


*Figure S26: TEM images and corresponding EDX analyses of* ***(a, b)*** *Au@TTT-TAPB and* ***(c, d)*** *Au@TTT-TAPB-S.*

### 4.12 Stability in acidic environment

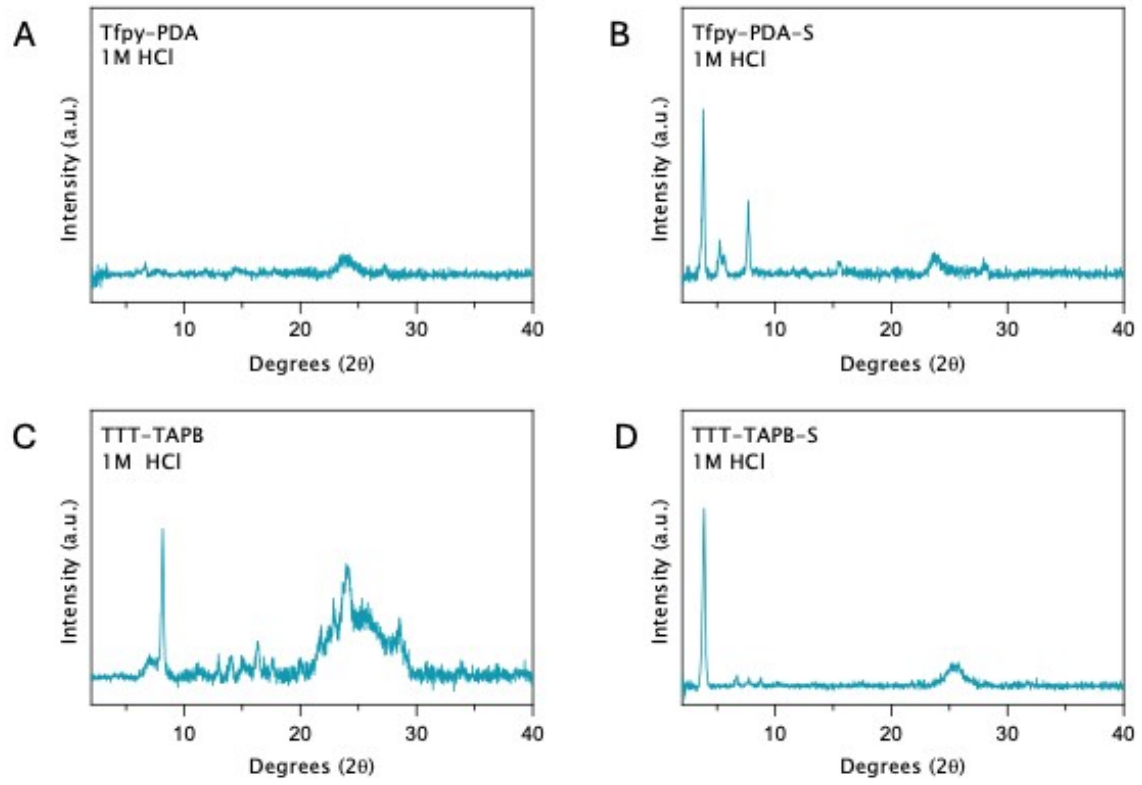


*Figure S27: PXRD of A) Tfpy-PDA, B) Tfpy-PDA-S, C) TTT-TAPB, D) TTT-TAPB-S after immersing COFs 24h in 1M HCl solution.*

## 5. Gold adsorption

### 5.1 General remarks

The gold solutions were prepared by dissolving the desired amount of $KAuCl_4$ into deionized water. The different concentrations were obtained by diluting the stock solution with deionized water. Furthermore, pH values were adjusted by adding a certain amount of a 6M stock solution of HCl. Adding other metal ions to the solutions was done by adding their respective metal chloride salts.

### 5.2 Gold adsorption isotherm

3 mg of COF was immersed in a 10 mL aqueous solution of $KAuCl_4$ of different concentrations (100 ppm, 250 ppm, 500 ppm, 750 ppm, 1000 ppm, 1250 ppm, 1500 ppm, 2000 ppm, and 3000 ppm). The mixture was stirred overnight in a 20 ml glass vial at room temperature. The filtrate was collected through a syringe filter and the concentration of the ions in the filtrate was analyzed with ICP-MS.

Langmuir adsorption model can be fitted to these isotherms.

Langmuir model $Q_e = Q_m \, . \, C_e / (K_L + C_e)$

with $Q_e$ = amount of gold adsorbed at equilibrium in mg/g

$C_e$ = concentration at equilibrium in ppm

$Q_m$ = maximum amount of gold per mass of adsorbent to form a complete monolayer

$K_L$ = constant describing the affinity of the binding sites

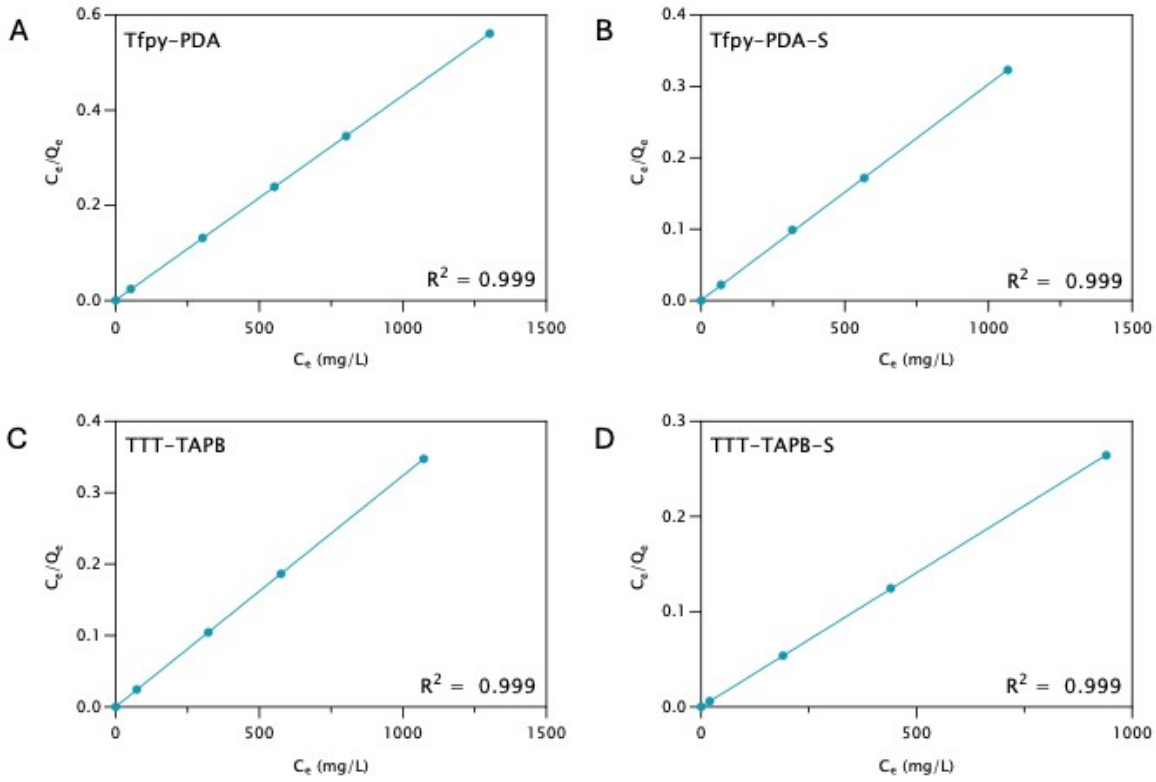


*Figure S28: Langmuir adsorption isotherm fitting curves for A) Tfpy-PDA, B) Tfpy-PDA-S, C) TTT-TAPB, D) TTT-TAPB-S.*

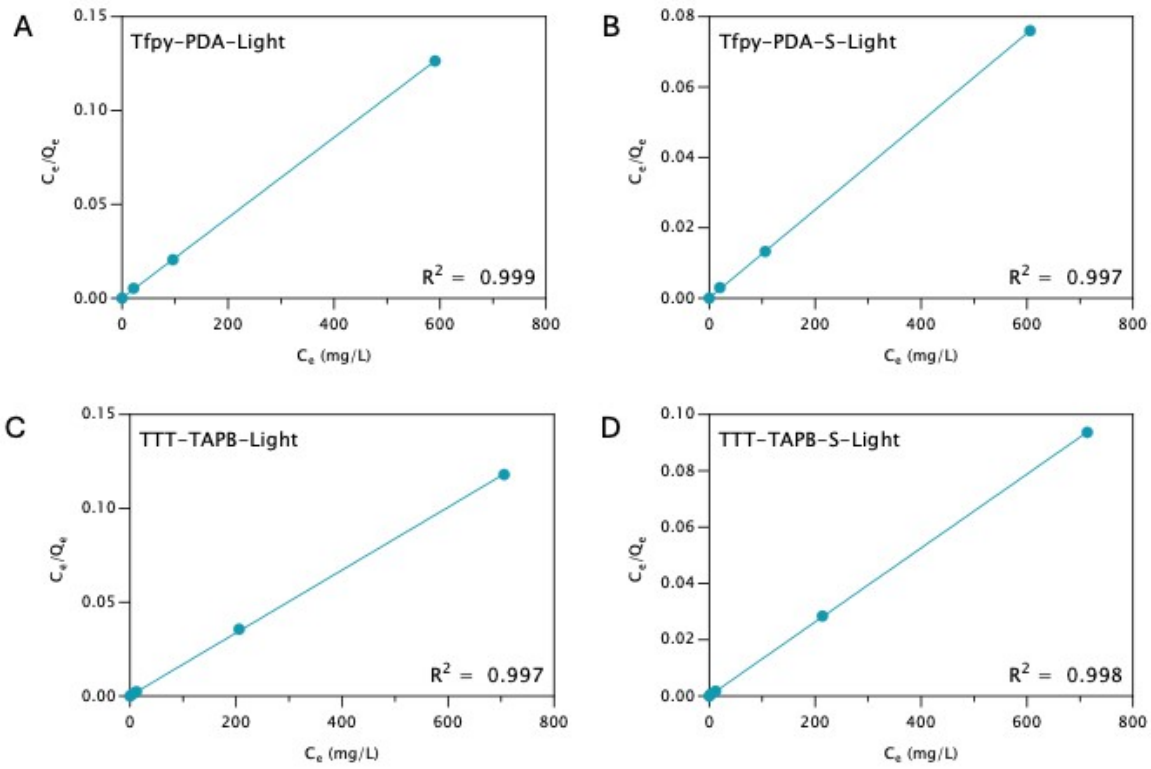


*Figure S29: Langmuir adsorption fitting curves for A) Tfpy-PDA, B) Tfpy-PDA-S, C) TTT-TAPB, D) TTT-TAPB-S under light irradiation.*

**Table S5: The adsorption capacities of the different COFs under dark and light conditions.**

| COF Material | $Q_m$,Dark (mg $g^{-1}$) | $K_L$,Dark (L $mg^{-1}$) | $Q_m$,Light (mg $g^{-1}$) | $K_L$,Light (L $mg^{-1}$) | Capacity Increase (%) |
|---|---|---|---|---|---|
| Tfpy-PDA | 2322 | 0.034 | 4680 | 0.121 | 102% |
| Tfpy-PDA-S | 3106 | 0.052 | 7980 | 0.204 | 157% |
| TTT-TAPB | 3088 | 0.164 | 5980 | 0.295 | 94% |
| TTT-TAPB-S | 3533 | 0.277 | 7620 | 0.382 | 115% |

### 5.3 Gold capture kinetics

The kinetics study was done by making a 100 ppm aqueous solution of gold ions with $KAuCl_4$. Then 10 mg of COF was immersed in 100 mL of the 100 ppm gold solution and stirred for 1 hour. Small amounts of solution were taken out at predetermined time intervals and filtered with a syringe filter (0.2 µm). The filtrate was analyzed with ICP-MS to determine the remaining gold concentration. The capture efficiency ($R_e$) is calculated from the following equation.

$R_e$ (%) = $[(C_0-C_e)/C_0] * 100$

With $C_0$ (mg/L) = initial concentration of $Au^{3+}$

$C_e$ (mg/L) = equilibrium concentration of $Au^{3+}$

Pseudo first-order model and pseudo-second order model was fitted to the kinetic data. The pseudo first-order equation can be expressed as $q_t=q_e\ (1-e^{(-k1t)})$ The pseudo-second order equation can be expressed as follows: $t/q_t = 1/k_2q_e^2 + t/q_e$.

With $q_t$ (mg/g) = adsorbed amount of Au(III) at time t.

$q_e$ (mg/g) = adsorbed amount of Au(III) at equilibrium.

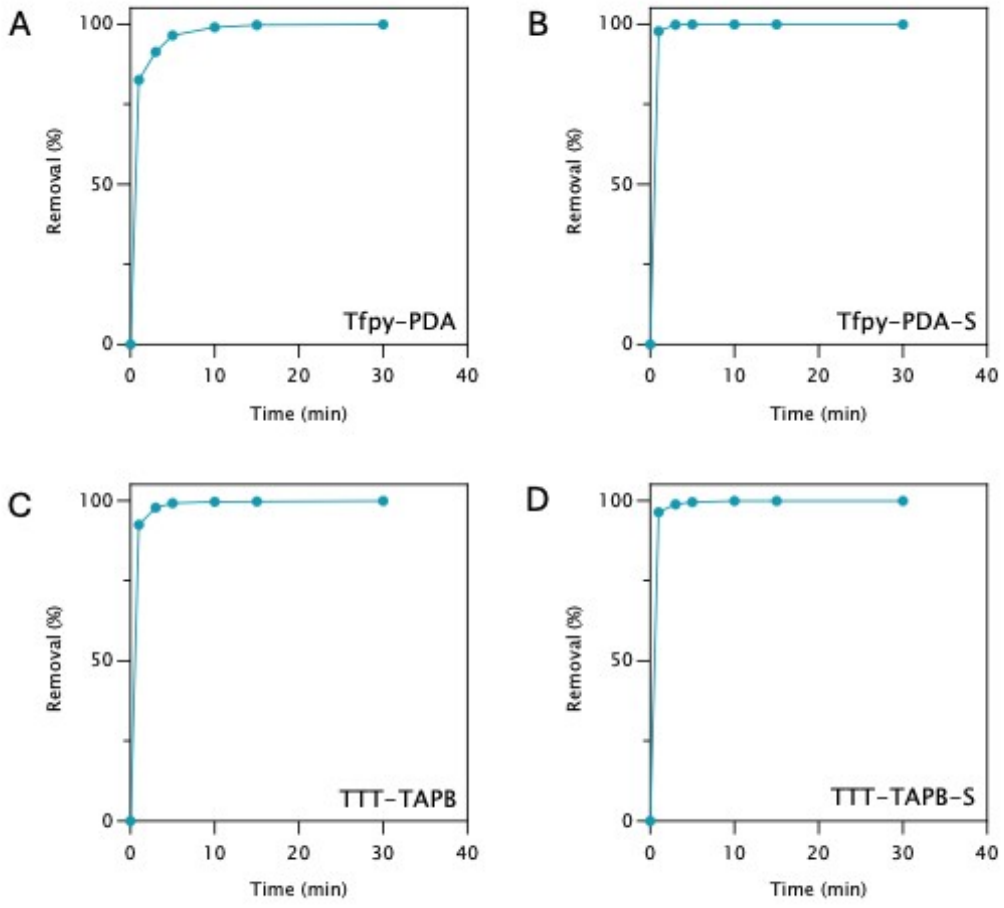


*Figure S30: Removal of 100 ppm of Au(III) in function of time on A) Tfpy-PDA, B) Tfpy-PDA-S, C) TTT-TAPB, D) TTT-TAPB-S.*

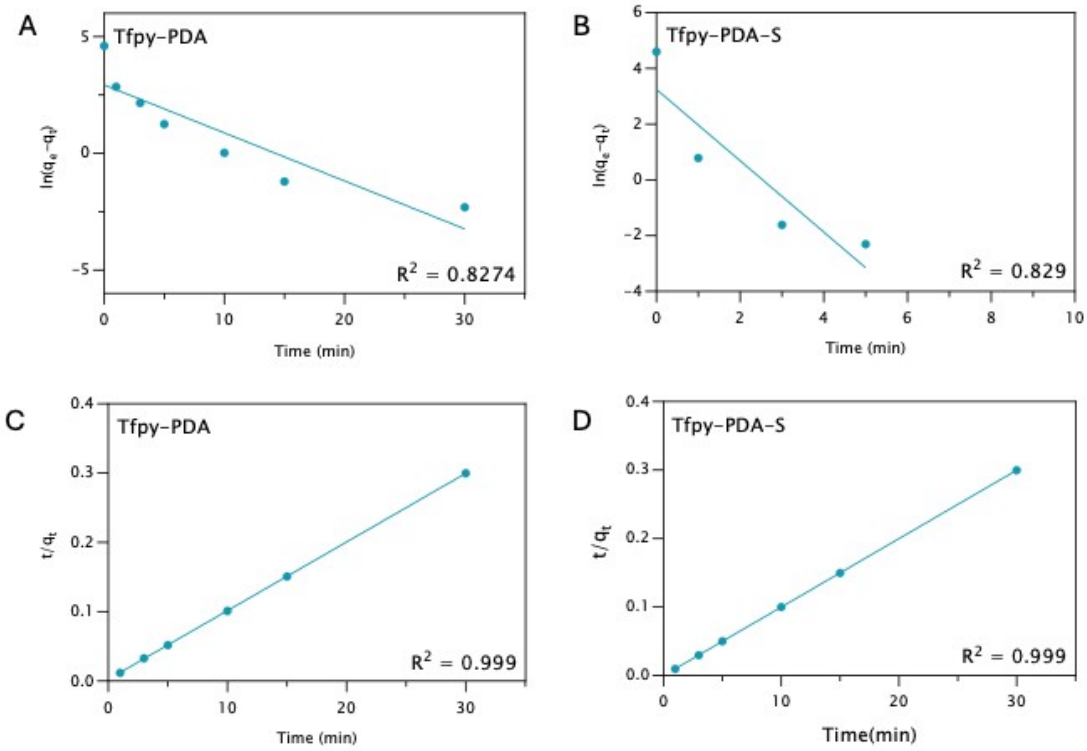


*Figure S31: Kinetic modelling of Au(III) adsorption with pseudo-first order model for A) Tfpy-PDA , B) Tfpy-PDA-S and pseudo-second-order model for C) Tfpy-PDA, D) Tfpy-PDA-S.*

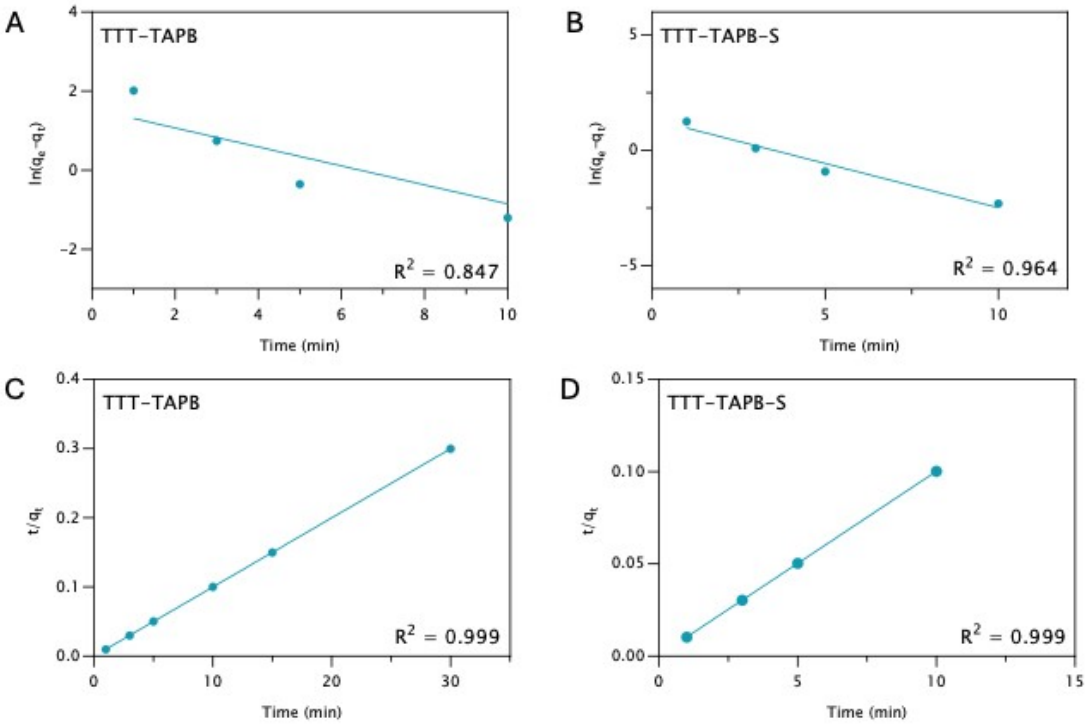


*Figure S32: Kinetic modelling of Au(III) adsorption with pseudo-first-order of A) TTT-TAPB, B) TTT-TAPB-S and pseudo-second-order of C) TTT-TAPB and D) TTT-TAPB-S.*

### 5.4 Gold adsorption selectivity

A mixture solution of $Cu^{2+}$, $Ni^{2+}$, $Al^{3+}$, $Ca^{2+}$, $Na^{+}$, $Zn^{2+}$, $Pb^{2+}$, $Pd^{2+}$ at a concentration of each metal ion (the corresponding chloride salts) of 100 ppm was prepared. To this solution 10 ppm of $Au^{3+}$ was added. Subsequently, 3 mg of the COF was added to 10 mL of the mixture solution and the mixture was stirred for 10 min at room temperature. The mixture was filtered through a 0.2 µm filter membrane. Finally, the filtrate was collected and its concentration was determined by ICP-MS.

To calculate the $K_d$ values of each ion: $K_d = (C_i - C_f / C_f) \times (V/m)$

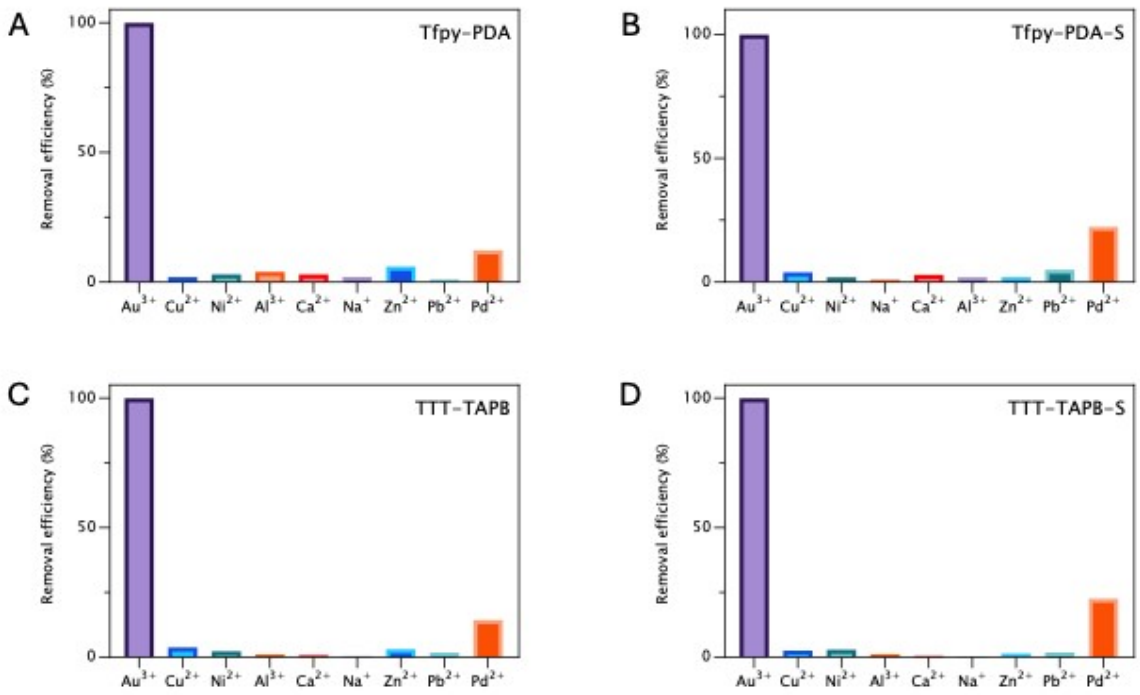


*Figure S33: Selectivity test by assessing the removal efficiency of different competing ions at 100 ppm and gold(III) ions at 10 ppm onto A) Tfpy-PDA, B) Tfpy-PDA-S, C) TTT-TAPB, D) TTT-TAPB-S.*

### 5.5 Gold adsorption performance at different pH

The effect of pH on gold adsorption was investigated from 2 to 12 by adjusting the pH of the solution with adding 6M of HCl or NaOH. Subsequently, 3 mg of COF was added to 10 mL of a 100 ppm solution of $Au^{3+}$ and stirred at room temperature for 2 hours. The mixture was filtered through a 0.2 µm filter membrane. Finally, the filtrate was collected and its concentration was determined by ICP-MS.

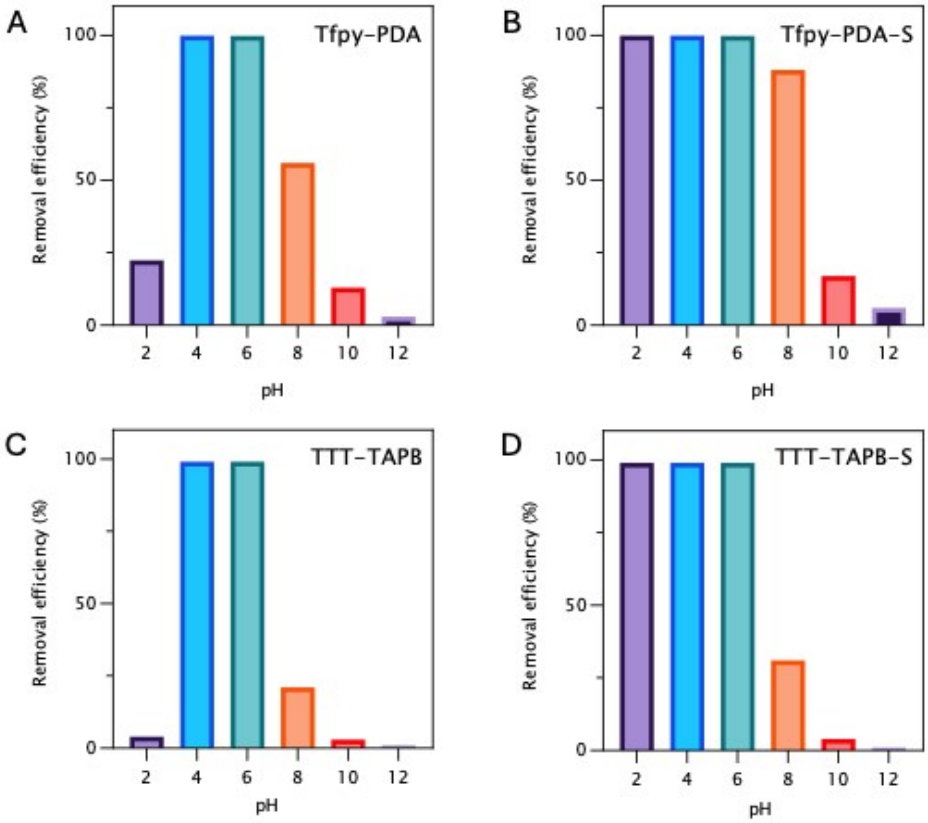


*Figure S34: Removal efficiency in function of pH in a 100 ppm Au(III) solution on A) Tfpy-PDA, B) Tfpy-PDA-S, C) TTT-TAPB , D) TTT-TAPB-S.*

### 5.6 Gold extraction from complex matrices

Different water samples were taken from the north sea, Blaarmeersen (lake water), and ground water (region Ghent, Belgium) and were spiked with 100 ppm Cu(II) and 100 ppm Ni(II) and 10 ppm Au(III). 5 mg of the COF added 10 mL of sea,lake, or ground water. The sample was stirred at room temperature for 2 hours. The mixture was filtered through a 0.2 μm filter membrane. Finally, the filtrate was collected and its concentration was determined by ICP-MS.

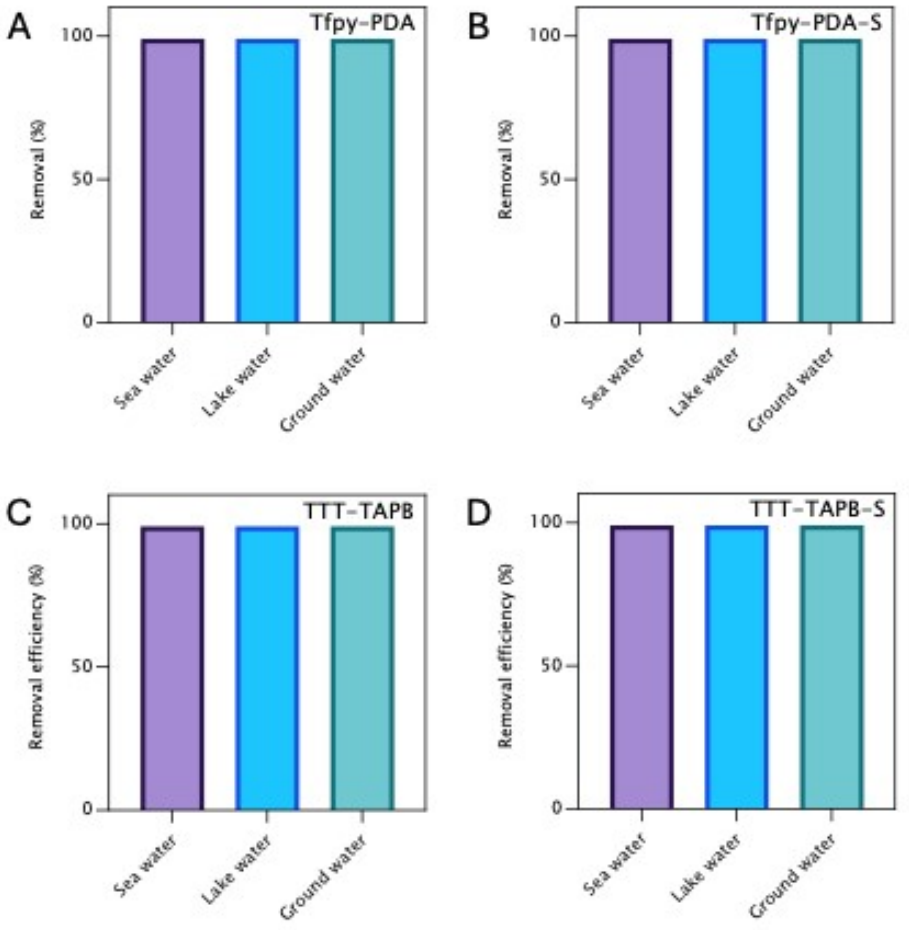


*Figure S35: Removal of 10 ppm Au(III) in different water matrices spiked with 100 ppm of Cu(II) and Ni(II) on A) Tfpy-PDA, B) Tfpy-PDA-S, C) TTT-TAPB, D) TTT-TAPB-S.*

## 5.7 Gold extraction from leaching solution of CPU (electronic waste)

For the recovery of the Au(III) from electronic waste an end-of-life CPU was immersed in an aqua regia solution consisting of 75 mL concentrated HCl and 25 mL of concentrated $HNO_3$ over 3 days. This aqua regia solution was further dilluted to pH 4. 10 mg of COF was added to 10 mL of the CPU solution and this solution was stirred for 1 hour at room temperature. After the adsorption, the mixture was filtered to separate the COF from the supernatant. The elemental composition of the supernatant was analyzed with ICP-MS and compared with the original CPU solution.

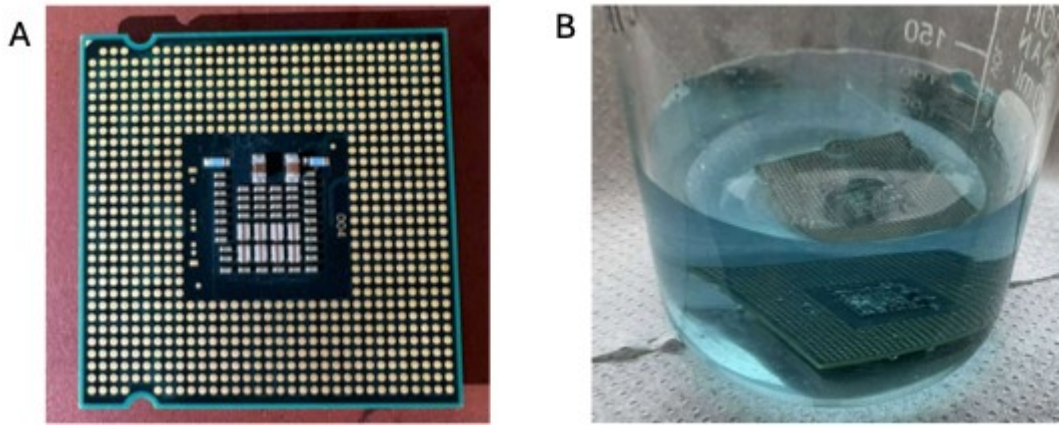


*Figure S36: A) Intel CPU processor, B) Leachate solution of CPU consisting of diluted aqua regia (pH= 4).*

## 5.8 Regeneration of COF after gold adsorption

After the adsorption of gold with 100 ppm solution of Au(III) solution, the COFs were filtered. 10mg of gold loaded COF were eluted in a 40 mL aqueous solution containing a 1:1 (V/V) ratio of 1M thiourea and 0.1M HCl and put in an ultrasonic bath for 30 min. The COF was filtered, washed with water and subsequently dried under vacuum. The gold ions in the resulting eluate was then chemically reduced with sodium metabisulfite ($Na_2S_2O_5$), which precipitated a fine, dark yellow gold powder.

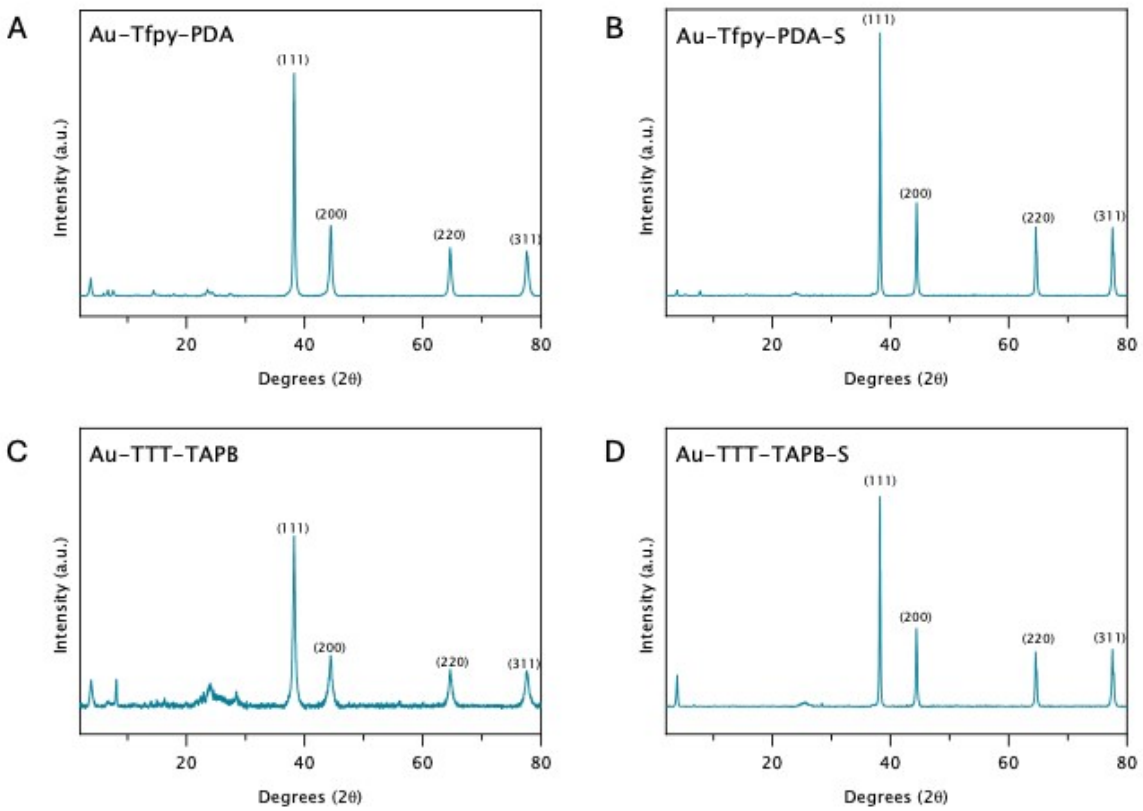


*Figure S37: PXRD after gold adsorption of A) Au-Tfpy-PDA, B) Au-Tfpy-PDA-S, C) Au-TTT-TAPB, D) Au-TTT-TAPB-S.*

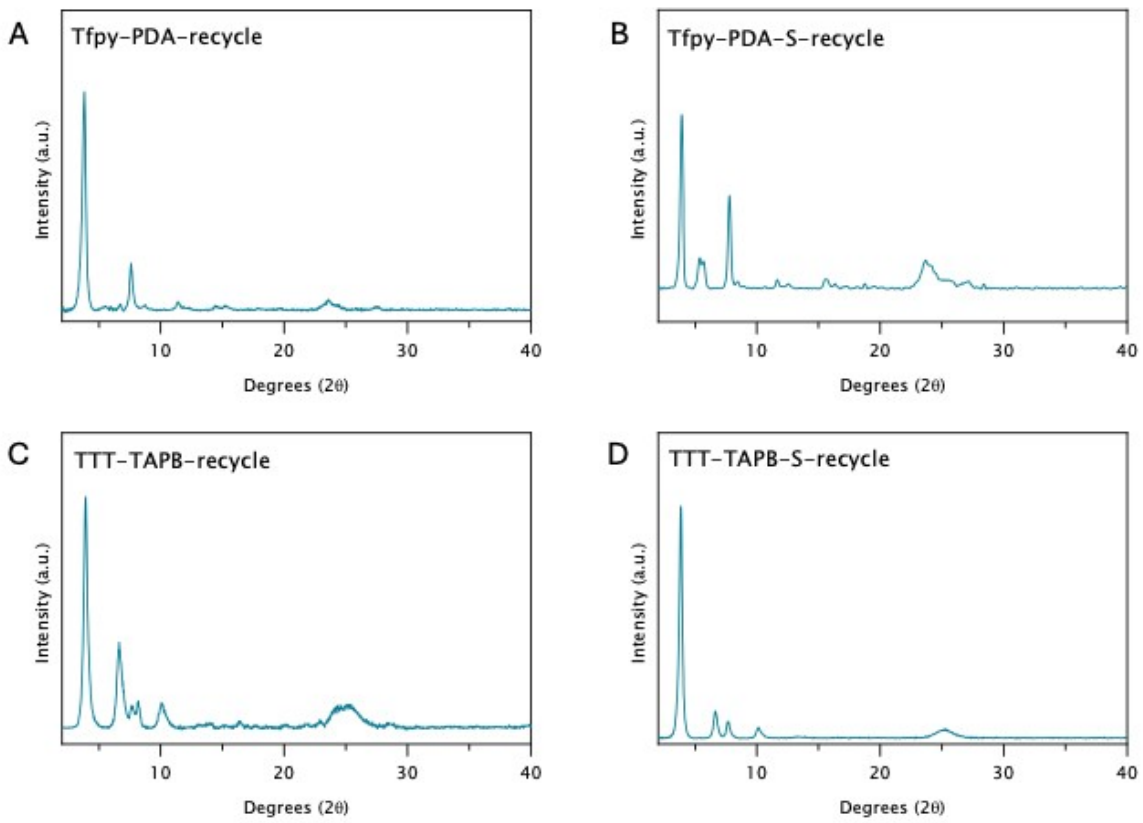


*Figure S38: PXRD of the recycled COFs after the first adsorption/recycle run with a 100 mg/L solution $AuCl_4^-$: A) Tfpy-PDA, B) Tfpy-PDA-S, C) TTT-TAPB, D) TTT-TAPB-S.*

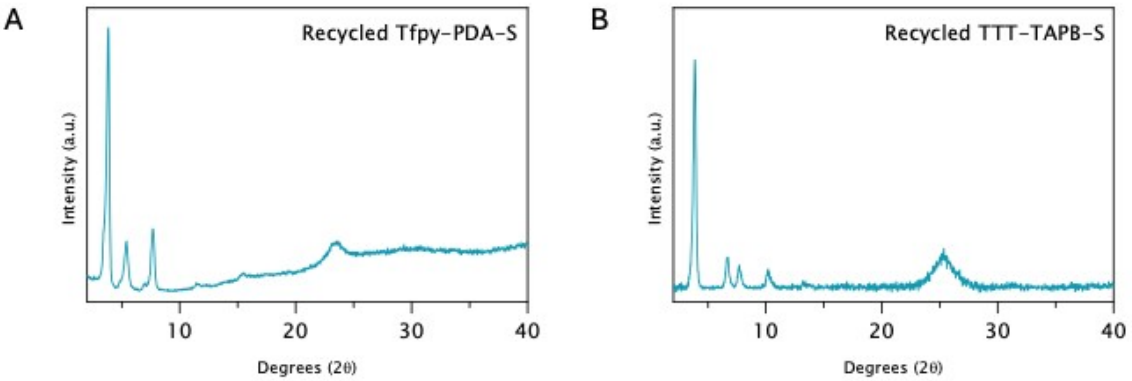


*Figure S39: PXRD of the recycled COFs after 5 cycles A)Tfpy-PDA-S, B)TTT-TAPB-S.*

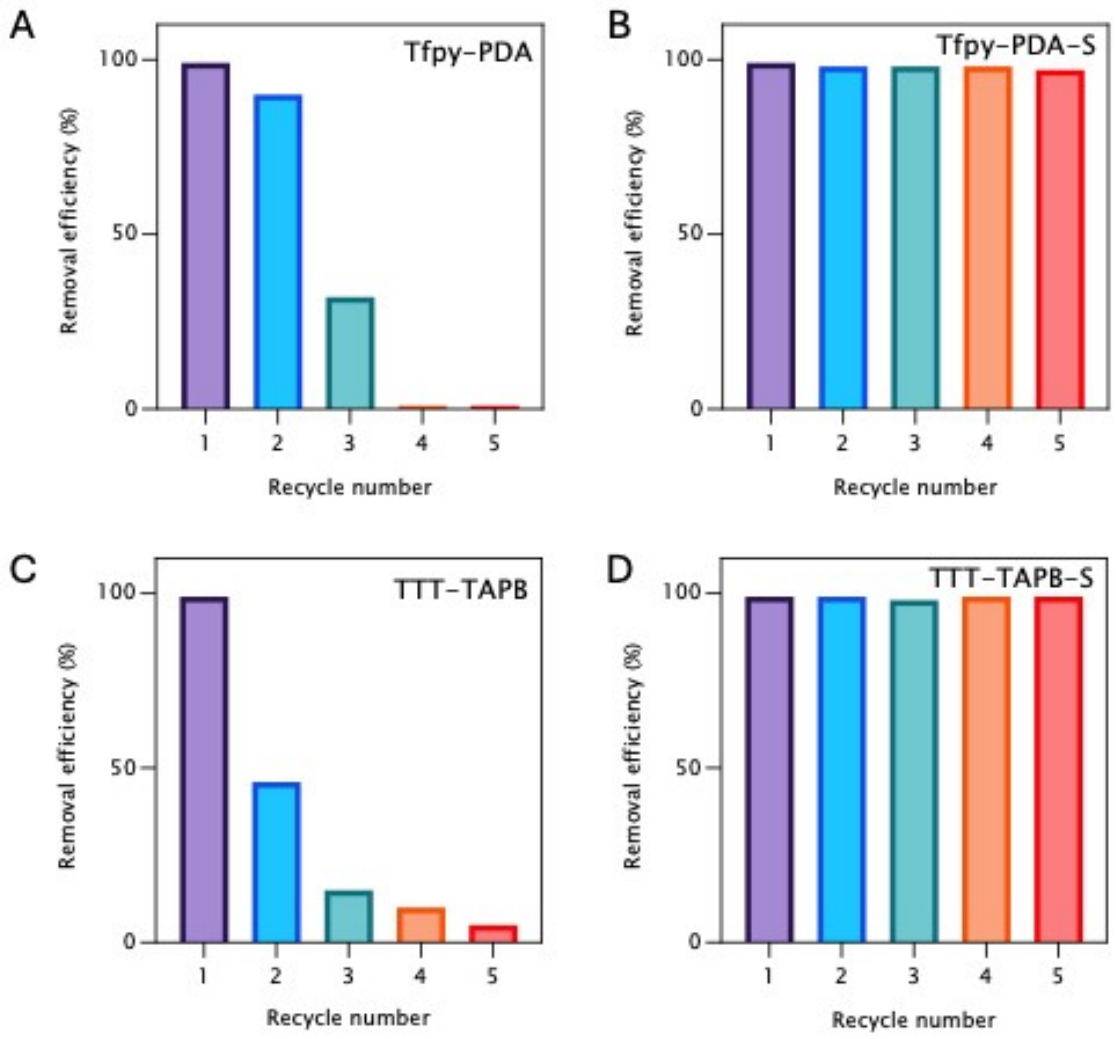


*Figure S40: Removal efficiency of 100 ppm $AuCl_4^-$ in function of recycle numbers with light irradiation of A) Tfpy-PDA, B) Tfpy-PDA-S, C) TTT-TAPB, D) TTT-TAPB-S.*

**5.9 $H_2O_2$ production**

5 mg of the COF was dispersed in 10 mL of degassed deionized water (degassed by bubbling 30 min of Ar) in a glass vial of 20 mL. Prior to the photocatalysis, the suspension was dispersed in a sonication bath for 10 min. Subsequently, the vial was irradiated by white LED (34W) lights for 3 hours and the reaction temperature was kept at 25°C. After certain time periods, an aliquot of the reaction mixture was filtered through a 0.22 μm syringe filter to remove the photocatalysts. The concentration of $H_2O_2$ was determined by using an UV-Vis spectrophotometer. The sample was mixed with a prepared $[Ti(OH)_3(H_2O)_3]^+_{(aq)}$ solution. The UV spectrophotometry $[Ti(O_2)OH(H_2O)_3]^+_{(aq)}$ color method follows the reaction, in which the colorless $[Ti(OH)_3(H_2O)_3]^+_{(aq)}$ reacts with $H_2O_2$ to generate a yellow peroxotitanium complex $[Ti(O_2)OH(H_2O)_3]^+_{(aq)}$ whose absorbance (A) can be measured at 410 nm (eq. S2).

$$TiOSO_{4(s)} + 5H_2O \leftrightarrow [Ti(OH)_3(H_2O)_3]^+_{(aq)} + HSO_4^-{}_{(aq)} \quad \text{(eq. S1)}$$

$$[Ti(OH)_3(H_2O)_3]^+_{(aq)} + H_2O_{2(aq)} \leftrightarrow [Ti(O_2)OH(H_2O)_3]^+_{(aq)} + 2H_2O \quad \text{(eq. S2)}$$

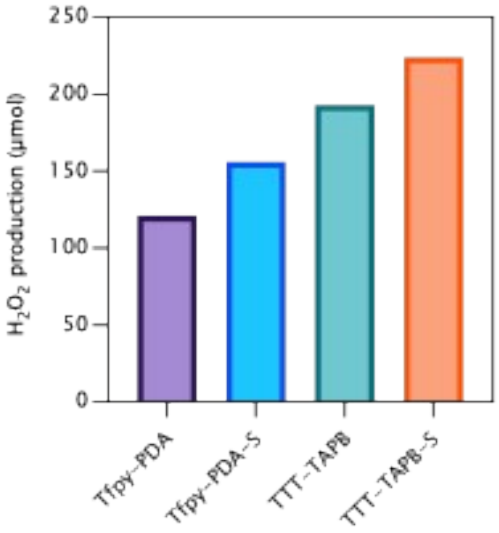


*Figure S41: $H_2O_2$ production amount during gold adsorption under dark conditions after 1 hour.*

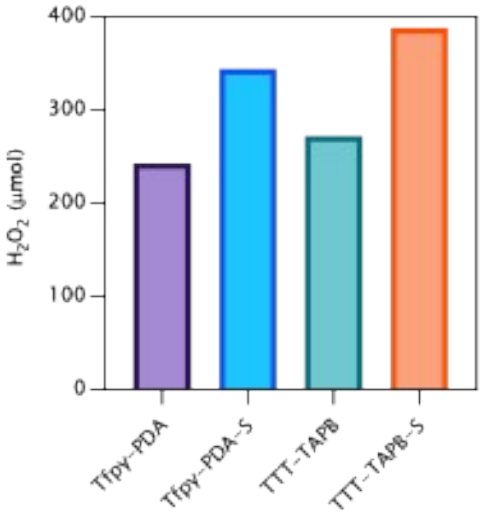


*Figure S42: Photocatalytic $H_2O_2$ production of each COF in water in an Ar atmosphere under light irradiation after 1 hour.*

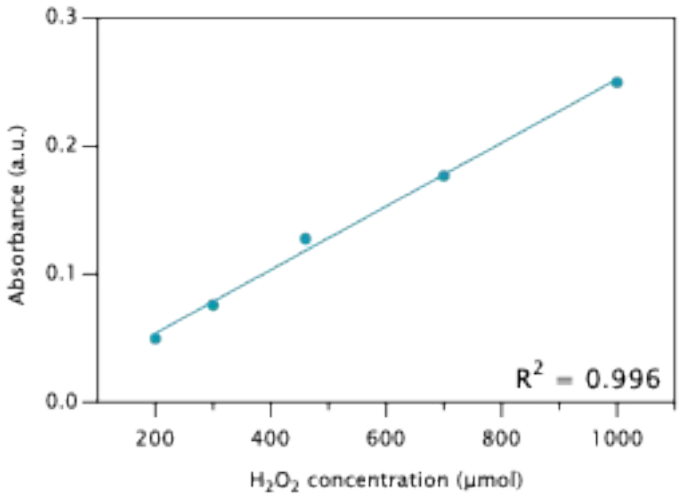


*Figure S43: Calibration curve of the UV-Vis measurements for $H_2O_2$ production.*

## 5.10 Comparison table of gold adsorbents

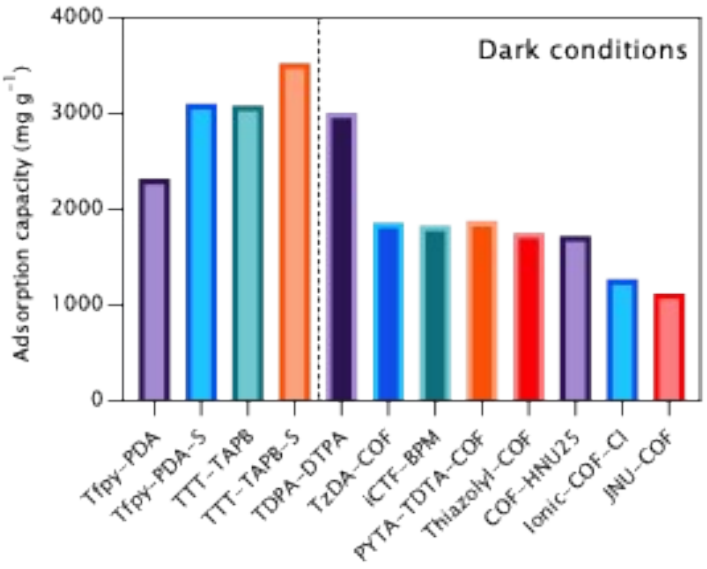


*Figure S44: Literature comparison of adsorption capacity onto COFs.*

The following COFs were compared from literature: TDPA-DTPA[4], TzDA-COF[5], iCTF-BPM[6], PYTA-TDTA-COF[7], Thiazolyl-COF[8], COF-HNU25[9], Ionic-COF-Cl[10], JNU-COF[11]

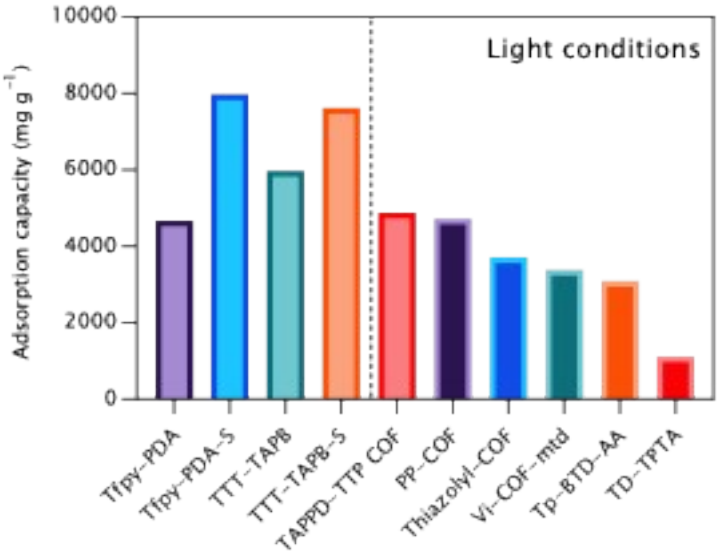


*Figure S45: Literature comparison of adsorption capacity onto COFs under light irradiation.*

The following COFs were compared from literature: TAPPD-TTP-COF[12], PP-COF[13], Thiazolyl-COF[8], Vi-COF-mtd[14], Tp-BTD-AA[15], TD-TPTA[16]

### 5.11 DFT binding energy diagrams

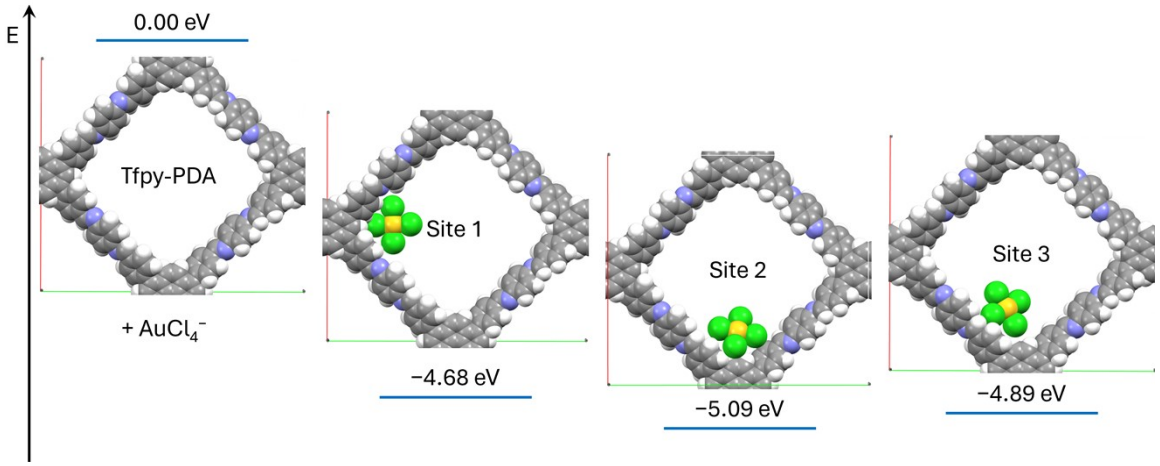


*Figure S46: Binding energies between $AuCl_4^-$ and Tfpy-PDA COF.*

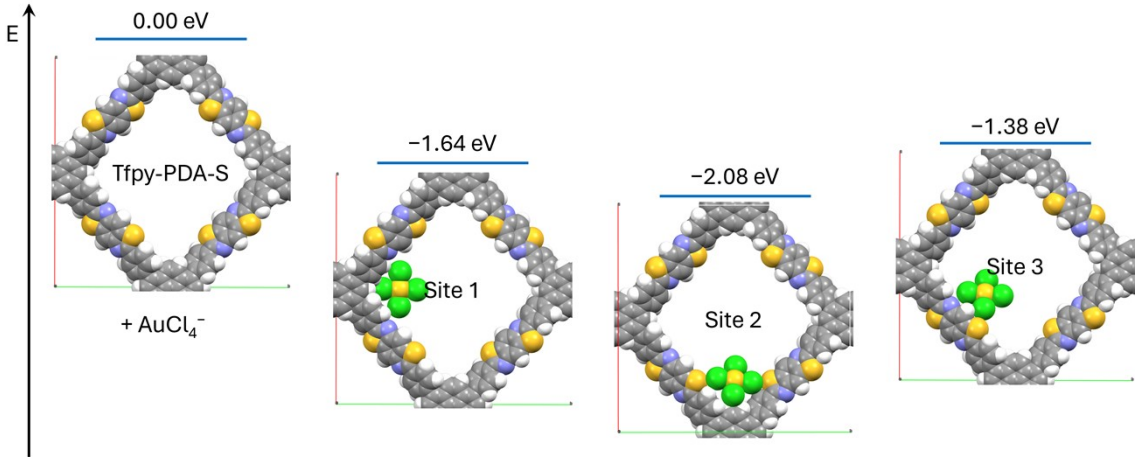


*Figure S47: Binding energies between $AuCl_4^-$ and Tfpy-PDA-S COF.*

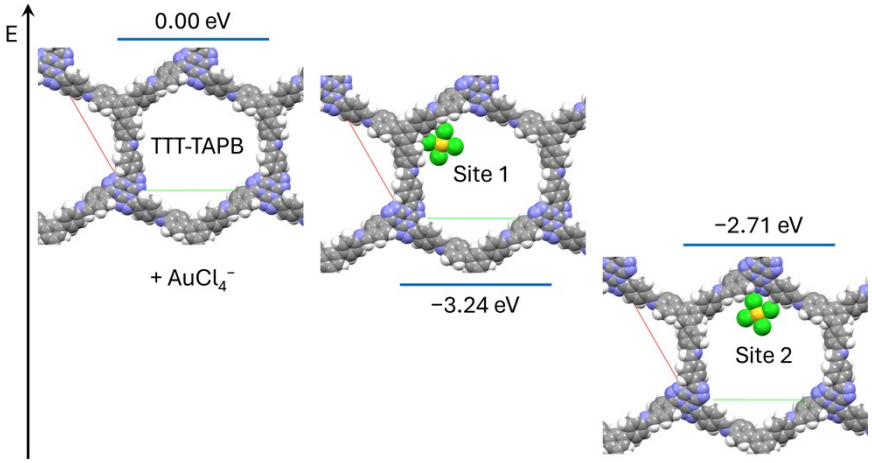


*Figure S48: Binding energies between $AuCl_4^-$ and TTT-TAPB COF.*

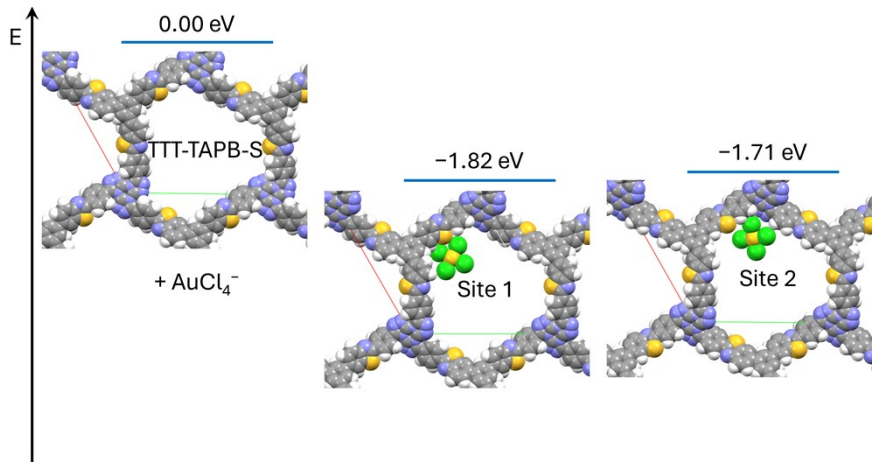


*Figure S49: Binding energies between $AuCl_4^-$ and TTT-TAPB-S COF.*

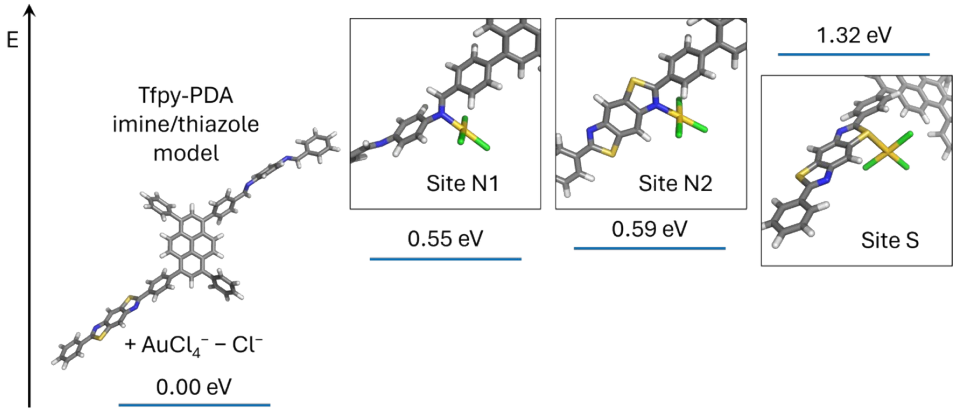


*Figure S50: Binding energies for chloride ligand exchange in water on $AuCl_4^-$ and different N and S binding sites on a model compound for Tfpy-PDA imine and thiazole COFs: N1 imine, N2 and S thiazole.*

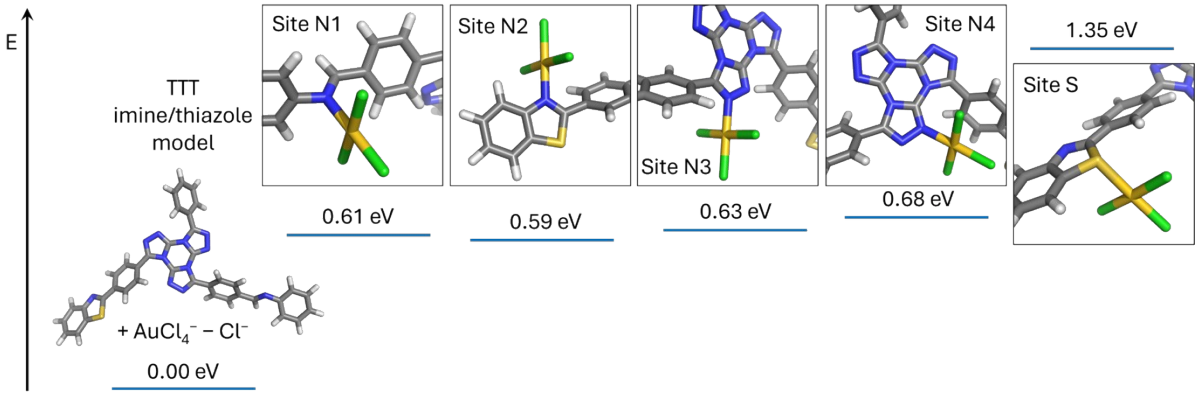


*Figure S51: Binding energies for chloride ligand exchange in water on $AuCl_4^-$ and different N and S binding sites on a model compound for COFs: N1 imine, N2 and S thiazole, N3 and N4 triazole.*

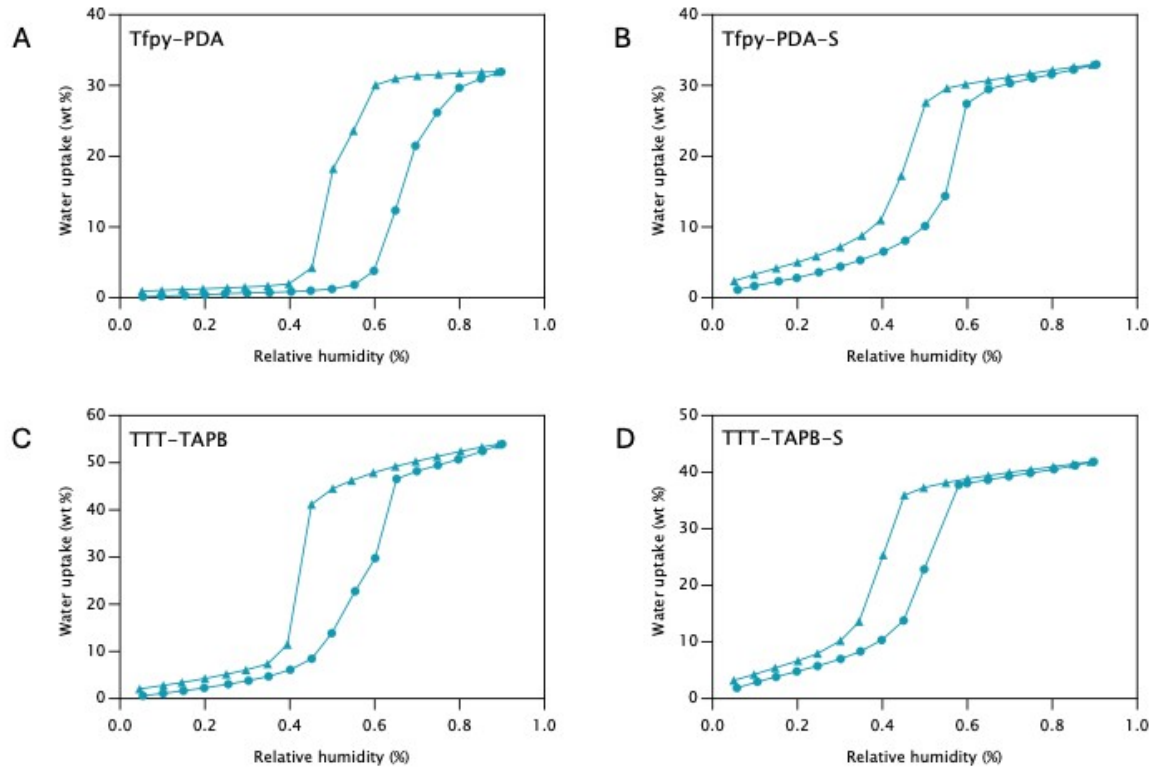


*Figure S52: Water sorption isotherms of A) Tfpy-PDA, B) Tfpy-PDA-S, C) TTT-TAPB, D) TTT-TAPB-S (circle: adsorption, triangle: desorption).*

## References


1 J. Tomasi, B. Mennucci and R. Cammi, *Chem Rev*, 2005, **105**, 2999–3094.

2 A. Laemont, G. Matthys, R. Lavendomme and P. Van Der Voort, *Angewandte Chemie International Edition*, 2024, **63**, e202412420.

3 Z. Zhang, Q. Zhang, Y. Hou, J. Li, S. Zhu, H. Xia, H. Yue and X. Liu, *Angewandte Chemie International Edition*, 2024, **63**, e202411546.

4 B. Ge, L. Yao, Y. Chen, H. Han, W. Jiao, X. Song, L. Sun and Z. Liang, *ACS Mater Lett*, 2024, **6**, 4230–4239.

5 S. Zhong, Y. Wang, T. Bo, J. Lan, Z. Zhang, L. Sheng, J. Peng, L. Zhao, L. Yuan, M. Zhai and W. Shi, *Chemical Engineering Journal*, 2023, **455**, 140523.

6 W. Wang, M. Wu, W. Xue, X. Zhao, Z. Fang, L. Nie, Y. Heng, H. Huang and C. Zhong, *Chemical Engineering Journal*, 2024, **483**, 149208.

7 M. Liu, D. Jiang, Y. Fu, G. Zheng Chen, S. Bi, X. Ding, J. He, B.-H. Han, Q. Xu and G. Zeng, *Angewandte Chemie International Edition*, 2024, **63**, e202317015.

8 Z. Huang, L. Guo, K. Yu, F. Gao, Y. Yang and F. Luo, *Chemical Communications*, 2024, **60**, 4950–4953.

9 J. Qiu, C. Xu, X. Xu, Y. Zhao, Y. Zhao, Y. Zhao and J. Wang, *Angewandte Chemie International Edition*, 2023, **62**, e202300459.

10 J. Zhao, Z. Qiao, Y. He, R. Zhang, H. Li, X. Song, D. Cao and S. Wang, *Angewandte Chemie International Edition*, 2025, **64**, e202414366.

11 H.-L. Qian, F.-L. Meng, C.-X. Yang and X.-P. Yan, *Angewandte Chemie International Edition*, 2020, **59**, 17607–17613.
12 B.-R. Huang, Y.-Z. Cheng, D. Jiang, B. Yuan, K.-F. Gao, Y.-Y. Duan, B.-W. Yao, D.-H. Yang, X. Ding and B.-H. Han, *Sep Purif Technol*, 2025, **366**, 132640.
13 Y.-Z. Cheng, X. Bao, D. Jiang, W. Ji, D.-H. Yang, X. Ding, X. Liu, Y. He and B.-H. Han, *Angewandte Chemie International Edition*, 2025, **64**, e202414943.
14 D. Jiang, Z.-L. Wang, Y.-Z. Cheng, Y.-X. Yu, H.-Y. Kong, X.-Y. Bian, X.-M. Dou, S.-L. Li, D.-H. Yang, X. Ding and B.-H. Han, *Chemical Engineering Journal*, 2024, **497**, 154212.
15 S. Yang, T. Li, Y. Cheng, W. Fan, L. Wang, Y. Liu, L. Bian, C.-H. Zhou, L.-Y. Zheng and Q.-E. Cao, *ACS Sustain Chem Eng*, 2022, **10**, 9719–9731.
16 Y. Wu, S.-H. Zeng, W. Xu, Y.-R. Chen, K. Liu, Y.-T. Dai, H.-Y. Wu and W.-R. Cui, *Sep Purif Technol*, 2024, **345**, 127408.